A STUDY OF THE HYDRODYNAMIC IMPACT LOADS ON A DIHEDRAL HYDROFOIL SUITABLE FOR SEAPLANE USE

RICHARD ALDEN HOFFMAN

ARTHUR CALVIN DERRICK

1957

MASTER'S THESIS

STEVENS INSTITUTE OF TECHNOLOGY

A STUDY OF THE HYDRODYNAMIC IMPACT LOADS ON A DIHEDRAL HYDROFOIL SUITABLE FOR SEAPLANE USE

A Thesis Submitted in Partial Fulfillment
of the Requirements for the Degree of
Master of Science

STEVENS INSTITUTE OF TECHNOLOGY

Submitted by Richard Alden Hoffman, LT. USN
Arthur Calvin Derrick, LT. USN

TABLE OF CONTENTS

ABSTRACT

An analysis of the use of planing data to predict impact loads of a dihedral hydrofoil suitable for seaplane installation is presented and compared with experimental model tests.

The experimental data verifies the theory very well for the prediction of maximum loads. No empirical correction factors are used and the theory agrees with experiment to an average error of 6.2% for the 47 runs analyzed. However, experimental time-to-peak tends to lag the theoretical, and the experimental draft time-history diverges from the computed after the point of maximum load.

One initial flight-path angle is considered for a comparison between the maximum loads predicted by these tests for a hydrofoil equipped seaplane and the maximum load expected of a chines-dry landing hull.

One initial flight-path angle is considered to compare the relative efficiency of the two models tested as energy absorbing devices.

In addition, a sample digital computer program useful in the application of the theory to the prediction of impact time-histories is presented.

This investigation, conducted at the Experimental Towing Tank, Stevens Institute of Technology, Hoboken, N.J., is the thesis submitted by the authors in partial fulfillment of the requirements for the degree of Master of Science.

NOTATION

M	Mass of impacting body
m_w	Virtual mass of displaced fluid
$\dot{z}_o$	Initial vertical velocity
$\dot{z}$	Instantaneous vertical velocity
$\ddot{z}$	Vertical acceleration
ρ	Mass density of water, 1.938 slugs/ft.^{3}
c	Wetted half-width
ℓ	Length of float
β	Wedge, dihedral or deadrise angle
m_s	Virtual mass of flow plane at step per unit distance in keel direction
τ	Geometric angle of trim
n_w	An area of fluid in a slice taken perpendicular to the keel
y	Displacement in a direction normal to the keel
$\dot{y}$	Velocity normal to the keel
$\ddot{y}$	Acceleration normal to the keel
y_s	Displacement of the step from origin in a direction perpendicular to the keel
x	Displacement in a direction parallel to the keel
$\dot{x}$	Velocity parallel to the keel
$\ddot{x}$	Acceleration parallel to the keel
x_s	Displacement of the step from the origin in a direction parallel to the keel

ρ Draft in y direction

ρ_s Draft of step in y direction

F_{ey} Elemental force normal to the keel

F_y Force normal to the keel

M_w Total mass affected by passage of body

$$M_w = \rho \cot \tau \int_0^{\rho_s} n_w \, d\rho$$

z Displacement in a vertical direction

μ $\frac{M_w}{M}$

F_z Force in vertical direction

μ' $\mu \cos^2 \tau$

V_H Horizontal velocity

Δt An arbitrary increment of time

γ_o Initial flight-path angle

$\frac{\partial \phi}{\partial t}$ Variation of the velocity potential with time in the general non-steady Bernoulli equation.

A Study of the Hydrodynamic Impact Loads on a Dihedral Hydrofoil Suitable for Seaplane Use

INTRODUCTION

The hydrofoil as a seaplane alighting device has received serious consideration as a possible means of relieving rough-water and high speed landing operational problems.

Compared to the conventional hull, the small area of the hydrofoil offers a considerable reduction of landing impact forces, while the fixed, relatively short hydrofoil chord limits center-of-pressure travel with a consequent reduction of undesirable pitching moments. To a large extent these particular advantages of the hydrofoil are shared with the hydroski, but the hydrofoil offers the additional advantage of lift/drag ratios superior to the ski, especially at low speeds.

Although the hydrofoil offers much promise for seaplane use, with the exception of a single experimental report of a classified proprietary nature, no studies of a general nature concerning its impacting properties are known.

The object of this work is to provide a rational foundation for the study and design application of impacting hydrofoils for seaplanes. To accomplish this end, an examination will be made of the use of planing data to compute impact loads and the

practicability of extending its use to the specific case of the hydrofoil; then to analyze and compare such analytical results with experimental model tests.

This investigation has been conducted by Lieutenents Richard A. Hoffman and Arthur C. Derrick, U.S. Navy, Naval Postgraduate School students at the Experimental Towing Tank, Stevens Institute of Technology, Hoboken, New Jersey. Special acknowledgement is due to Professor B.V. Korvin-Kroukovsky, Mr. Daniel Savitsky, Mr. P. Ward Brown and Mr. Robert Van Dyck of the Experimental Towing Tank Staff for their most helpful interest and guidance in this work. Thanks are also in order to all of the other members of the staff who so freely gave of their assistance, experience and advice during this investigation.

EXAMINATION OF THE USE OF PLANING DATA TO COMPUTE HYDROFOIL IMPACT LOADS

Historical Background

The earliest impact theories for the landing of seaplanes were based on the work of von Karman (Ref. 1) in which he considered a wedge shaped body dropped vertically into a horizontal water surface. With the assumption that momentum was transferred to a hypothetical associated mass of water attached to the seaplane and that the total momentum of the system remained constant, von Karman was able to write the momentum equation:

$$M\dot{z}_o = M\,\dot{z} + m_w\,\dot{z} \qquad (1)$$

where M - mass of the impacting body

m_w - virtual mass of displaced fluid

$\dot{z}_o$ - initial vertical velocity

$\dot{z}$ - instantaneous vertical velocity

With the further assumption of two dimensional flow in planes normal to the keel, von Karman considered at each instant the virtual mass is equal to the mass of water contained in a semi-cylinder of length equal to the length of the float and of diameter equal to the width of the wedge at the water surface (Fig. 1). This expression for the virtual mass substituted into equation (1) led to the force equation:

$$F_z = \frac{\dot{z}_o \, \rho \pi c^2 \ell \cot \beta}{3 \left(1 + \frac{\rho \pi c^2 \ell}{2M}\right)} \qquad (2)$$

where c - wetted half width

ℓ - length of body

Subsequently Wagner (Ref. 2) took into account the wave rise at the wedge surface and defined the diameter of the semi-cylinder of virtual mass on the basis of deadrise and draft (Fig. 1a); and Pabst (Ref. 3) introduced an aspect ratio factor to account for end losses in approximating oblique impact on the basis of the two-dimensional calculation.

Mayo (Ref. 4) in 1945 analyzed the basic von Karman theory and concluded it erred in assuming the total momentum of the system remained constant in that it did not account for momentum transfer onto the wake. Mayo pointed out that a more realistic force equation would be

$$F_y = \frac{d}{dt}(m_w \dot{y}) + m_s \dot{x} \dot{y} \qquad (3)$$

where $\dot{y}$ - velocity normal to keel

$\dot{x}$ - velocity parallel to keel

m_s - virtual mass of flow plane at step per unit distance in keel direction

in which the rate at which momentum is imparted to the downwash is included.

Mayo, using equation (3), was able to apply the von Karman theory to chines dry oblique impact by imagining the fluid beneath the wedge divided into slices of length dx by planes drawn normal to the keel. As the wedge moves through these slices, the flow in each slice is assumed to be identical with the flow in the case of the wedge dropped vertically. By assuming the fluid in each slice to be independent of the motion in adjacent slices, the total force on the wedge is equal to the sum of the forces of all the slices acting on the wedge plus the rate at which momentum is imparted to the downwash by flow planes sliding off at the step.

Mayo pointed out that in planing the first term of equation (3) is 0 and the hydrodynamic force is equal to the last term and therefore planing data might be used to evaluate the momentum of the flow in the normal cross sections.

Subsequently, in 1948 Steiner (Ref. 5) followed Mayo's approach to obtain correlation between planing data and one of the virtual mass expressions, using limited data mostly confined to the chines dry case. In 1951 Smiley (Ref. 6) used planing to obtain a correlation between planing and impact for a flat plate, obtaining an impact pressure coefficient in terms of an "equivalent planing velocity".

With the advent of heavily loaded high length-beam ratio hulls which immersed chines in landing and of flat bottom skis, certain inherent weaknesses of the classic theory precluded its

use for these modern applications. For example: for a flat bottom the force equation (2) yields an infinite force; while for the case of chines wet impact, the virtual mass becomes constant at chine immersion and does not increase with increasing draft.

In 1952 Schnitzer (Ref. 7) treated the case of chines wet impact by constructing a composite deflected mass from the deflected (virtual) mass apparent at chine immersion plus a deflected mass derived from Bobyleff's theory of the flow about a two-dimensional V-shape of finite width. However, Schnitzer's theory was lacking somewhat in generality in that it attempted to absolutely define the geometry of the virtual mass.

Also in 1952 Smiley (Ref. 8) presented an analysis for the landing impact in which the landing loads and motions are expressed in terms of the planing properties of the body. However, Smiley reverted to an empirico-theoretical virtual mass expression at chine immersion.

In 1954, Brown (Ref. 9) exploited to the full the concept that impact characteristics may be predicted with the use of planing data, avoiding the unverifiable definition of the geometry of the virtual mass.

Brown's approach is especially attractive for the computation of impact loads on such complicated shapes as hydrofoils and skis, since it is unhampered by empirico-theoretical expressions for virtual mass. In its published form however, the derivation

of Brown's theory breaks down when the leading edge of the body becomes wetted as in an impacting hydrofoil. During the course of this work Mr. Brown became associated with the Experimental Towing Tank and through his cooperation the derivation was modified so that the theory is applicable to any impacting body for which planing data is known.

Because of its logical simplicity and its applicability to any planing body, Brown's approach is the one followed in this analysis and the revised derivation is discussed below.

Seaplane Impact Theory as Applied to the Hydrofoil

The following analysis considers the impact of a straight-keeled planing body of arbitrary cross section.

The following assumptions are made:

1. Trim, τ, remains constant throughout the impact.
2. Inertia forces predominate.
3. The body is a weightless mass, weight supported by wing lift.
4. The virtual mass M_w, is some function of the draft.

Consider the impacting body shown in Fig. 2. In the fixed plane AA' a cross sectional area of water n_w is influenced by the passage of the body.

$$\left.\begin{array}{l}\text{The momentum of the fluid in the} \\ \text{element } n_w \text{ normal to the keel}\end{array}\right\} = \rho\, n_w\, \dot{y}_s\, \delta x \qquad (4)$$

The area n_w is considered to be a function of the draft ζ, since in a body of known geometry at fixed trim, any cross-sectional area may be determined if the draft is known. When the body has passed through AA', the momentum in the element is considered as shed to the wake. This concept is discussed more fully in Monaghan (Ref. 10).

$$\left.\begin{array}{l}\text{The rate of change of momentum}\\ \text{in an element fixed in space}\end{array}\right\} = \frac{d}{dt}(\rho\, n_w\, \dot{y}_s\, \delta x)$$

$$= \rho\, \delta x(\ddot{y}_s n_w + \dot{y}_s \frac{dn_w}{dt}) \quad (5)$$

but $$\frac{dn_w}{dt} = \frac{dn_w}{d\zeta} \cdot \frac{d\zeta}{dt}$$

and from Fig. 2 $\zeta = y_s - x \tan \tau$

and since the plane is fixed x is constant

$$\therefore \dot{\zeta}_s = \dot{y}_s$$

and (5) becomes $$= \rho\, \delta x\, (\ddot{y}_s\, n_w + \dot{y}_s^{\,2}\, \frac{dn_w}{d\zeta}) \quad (6)$$

Since $$\left.\begin{array}{l}\text{Rate of change of}\\ \text{momentum in an}\\ \text{element}\end{array}\right\} = \left\{\begin{array}{l}\text{Force exerted on}\\ \text{body by element}\end{array}\right.$$

$$F_{ey} = \rho\, \delta x\, (\ddot{y}_s\, n_w + \dot{y}_s^{\,2}\, \frac{dn_w}{d\zeta}) \quad (7)$$

This determines the elemental force acting on the body in a fixed plane. To determine the total force acting on the body at any one instant of time, consider the body's position, velocity and acceleration to be instantaneously fixed. Now let the

previously fixed plane move along the body, recalling as x varies, $\mathcal{S}$ varies and with $\mathcal{S}$, n_w.

Since $\mathcal{S} = y_s - x \tan\tau$, under the above conditions $d\mathcal{S} = -\tan\tau\, dx$ and

$$F_y = \int_{x_s}^{x_s+L} (\rho\, \ddot{y}_s\, n_w + \rho\, \dot{y}_s^{\,2} \frac{dn_w}{d\mathcal{S}})\, dx$$

$$= \rho\, \ddot{y}_s \cot\tau \int_0^{\mathcal{S}_s} n_w\, d\mathcal{S} + \rho\, \dot{y}_s^{\,2} \cot\tau \int_0^{\mathcal{S}_s} \frac{dn_w}{d\mathcal{S}}\, d\mathcal{S} \qquad (8)$$

Now define M_w, the total mass effected by the passage of the body as:

$$M_w = \rho \cot\tau \int_0^{\mathcal{S}_s} n_w d\mathcal{S}$$

$$\therefore \frac{dM_w}{d\mathcal{S}_s} = \rho \cot\tau \int_0^{\mathcal{S}_s} \frac{dn_w}{d\mathcal{S}}\, d\mathcal{S} \qquad (9)$$

Equation (9) may not be readily apparent, but it may be proved by a series expansion of n_w as a function of $\mathcal{S}$.

Therefore, substituting (9) into (8)

$$F_y = \ddot{y}_s\, M_w + \dot{y}_s^{\,2} \frac{dM_w}{d\mathcal{S}_s} \qquad (10)$$

From Fig. 2, $\mathcal{S}_s = z \sec\tau$

$$d\mathcal{S}_s = \sec\tau\, dz$$

and equation (10) becomes

$$F_y = \ddot{y}_s M_w + \dot{y}_s^2 \frac{dM_w}{dz} \cos \tau \qquad (11)$$

From Newton's Second Law

$$F_y = - M \ddot{y}_s$$

$$\therefore - M \ddot{y}_s = \ddot{y}_s M_w + \dot{y}_s^2 \frac{dM_w}{dz} \cos \tau$$

$$- \ddot{y}_s = \dot{y}_s^2 \frac{dM_w}{dz} \cos \tau \frac{1}{M(1 + \frac{M_w}{M})} \qquad (12)$$

Define $\frac{M_w}{M} = \mu$, then $\frac{dM_w}{dz} = M \frac{d\mu}{dz}$

Substituting in (12)

$$- \ddot{y}_s = \dot{y}_s^2 \frac{d\mu}{dz} \cos \tau \frac{1}{(1 + \mu)} \qquad (13)$$

Determination of $\frac{d\mu}{dz}$ and μ

Consider planing as a special case of impact, Fig. 3. In this case

$$\ddot{y}_s = 0 \qquad F_z = F_y \cos \tau$$

$$\dot{y}_s = V_H \sin \tau \quad \text{where } V_H \text{ is the horizontal planing velocity}$$

and substituting in (11) yields

$$F_z = V_H^2 \sin^2 \tau \cos^2 \tau \, M \frac{d\mu}{dz}$$

$$\therefore \quad \frac{d\mu}{dz} = \frac{F_z \, g}{V_H^2 \sin^2 \tau \cos^2 \tau \, \Delta_o} \tag{14}$$

$$\mu = \frac{g}{V_H^2 \sin^2 \tau \cos^2 \tau \, \Delta_o} \int_o^z F_z \, dz \tag{15}$$

The constant of integration is zero since $\mu = 0$ at $z = 0$

Thus the virtual mass ratio μ is defined in terms of the integrated lift/draft curve and constants.

In order to change the equation of motion (13) which is in terms of velocities and accelerations normal to the keel to the more useful terms of vertical velocities and accelerations (as are measured in the towing tank), substitute in (11)

$$F_y \cos \tau = F_z$$

$$\dot{y}_s = V_H \sin \tau + \dot{z} \cos \tau$$

$$\ddot{y} = \ddot{z} \cos \tau$$

$$\therefore \quad F_z = \ddot{z} \cos^2 \tau \, M_w + (V_H \sin \tau + \dot{z} \cos \tau)^2 \frac{dM_w}{dz} \cos^2 \tau \tag{16}$$

Since $F_z = - M_w \ddot{z}$, combining with (16) and (14) and rearranging yields

$$- \ddot{z} = F_z \left[\frac{V_H \sin \tau + \dot{z} \cos \tau}{V_H \sin \tau} \right]^2 \frac{1}{M(1 + \mu \cos^2 \tau)} \tag{17}$$

Letting $\mu' = \mu \cos^2 \tau$ yields

$$-\ddot{z} = F_z \left[\frac{V_H \sin \tau + \dot{z} \cos \tau}{V_H \sin \tau} \right]^2 M \left(\frac{1}{1 + \mu'} \right) \qquad (18)$$

The resulting non-linear equation (18) does not lend itself to a closed solution, therefore a step-by-step integration is necessary to compute the time history of impact.

Step-by-Step Integration of Equation of Motion (18)

The purpose of this integration is to determine the time-history of hydrofoil impact after striking the water under known initial conditions. During this impact the trim is assumed to remain constant, as is the horizontal velocity.

The horizontal velocity, trim angle, initial vertical velocity, weight of the body and a curve of steady state planing lift versus draft for the horizontal velocity of impact are known. Then to perform the integration the only quantity needed is a time interval (Δt) small in respect to the time from contact to maximum load.

If zero time is the instant of contact, the average draft during the first interval is

$$d_{av_1} = \frac{\dot{z}_o \, \Delta t}{2}$$

Then from a curve of planing lift versus draft for the foil, the lift (F_z in equation 18) for the average draft is determined

and from an integrated plot of F_z versus draft, the quantity $\int_o^z F_z \, dz$ used in the determination of u' is found.

To compute the acceleration, the planing lift is multiplied by the quantity

$$\frac{g}{\Delta_o}\left[\frac{V_H \sin\tau + \dot{z}_o \cos\tau}{\dot{x}\sin\tau}\right]^2 \frac{1}{1 + \frac{g}{\Delta_o V_H^2 \sin^2\tau}\int_o^z F_z \, dz}$$

all quantities of which are now known.

The vertical velocity at the end of the interval is

$$\dot{z}_1 = \dot{z}_o - \ddot{z}\,\Delta t$$

and the draft is

$$d_1 = \frac{\dot{z}_o + \dot{z}_1}{2}\Delta t$$

Using $\dot{z}_1$ and d_1 as initial conditions, the average draft for the next interval would be

$$d_{av_2} = d_1 + \frac{\dot{z}_1 \Delta t}{2}$$

and the procedure is repeated.

The most efficient manner to accomplish the integration is in tabular form, a sample of which is given as Table I. However, even at best the step-by-step integration is a tedious and time-consuming task, and since each result is dependent upon the previous one, it is a process in which errors accumulate.

An examination of Table I reveals that the step-by-step integration is in a form to be easily programmed for a digital computer. This was done for the ELECOM 100, and a sample flow chart easily adaptable to any digital machine is included as Table II.

Computation of Impact by Digital Computer

The sample flow chart is so constructed as to be useful for the determination of impact time histories of any arbitrary bodies for which planing data is known.

The main program is standard and need not be altered if the lifting characteristics of the body are changed. The F_z vs. z and $\int_o^z F_z\, dz$ vs. z functions are in subroutines which may be changed with comparative ease.

With this sample program the only inputs needed in addition to the above subroutines are V_H, $\dot{z}_o$, $\sin\tau$, $\cos\tau$, Δ_o, g, Δt, 1 and 2. Therefore numerous runs may be computed in a very short time.

All theoretical curves except for the run of Table I were computed using this program.

EXPERIMENTAL INVESTIGATION

Purpose

While the planing analogy as a means of computing impact loads has become well established in recent years, Refs. 5 through

9 and 11, all known experimental data analyzed by this technique has concerned hulls or skis of low aspect ratio and a dry leading edge. Although intuitively it might be expected that the analogy would hold for any planing body for which the lift coefficients are known, the large aspect ratio and submerged condition of the hydrofoil make it so different from the bodies previously studied as to indicate a definite need for experimental data to verify the applicability of the use of planing data to compute impact loads. To this end the facilities of the seaplane tank, Experimental Towing Tank, Stevens Institute of Technology were employed.

Equipment and Procedure

Two hydrofoil models made from half-hard brass bar stock were used for the tests. The first model consists of a center-supported V-shaped hydrofoil with a constant chord of one inch and a length of each arm of five inches. The dihedral of the arms is 30 degrees from the horizontal. The bottom of the foil is flat with sharp leading and trailing edges. The center support is 15 inches long and sharp-edged to prevent excessive drag from developing as a result of spray. Bracing from the foil tips to the center strut were added to insure rigidity. See Fig. 4.

The second hydrofoil is the same except that the chord, instead of being constant, has a taper ratio of 1:2 with a one inch chord at the center and a two inch chord at the ends. See Fig. 4.

The tests utilized the Tank 3 "Nutcracker" apparatus with a

Schaevitz type AB-2 accelerometer with "damped natural frequency" on the order of 90 cycles per second and approximately 0.7 critical damping. The standard Tank 3 speed and recording equipment was used in connection with two Hathaway oscillograph recorders for time-variable measurements.

The readings of heave and acceleration are picked up by and transmitted by means of Schaevitz electro-mechanical differential induction transformer units which give approximately linear response of output voltages to input mechanical deflections.

The Tank 3 "Nutcracker" apparatus (Figs. 5, 6) consists of a pole free to move vertically through two collars housing low-friction ball bearings but limited from horizontal rotation by means of a pivoted arm and elbow linkage. This apparatus has a built-in Schaevitz unit to measure heave of the pole by means of a string wound around a pulley on a worm gear. A solenoid-controlled heave lock device is built onto the "Nutcracker". In the tests this device was tripped electrically as soon as the carriage reached a predetermined steady speed energizing the solenoid which pulled a pin out of the pole and allowed the model to drop into the water. The "Nutcracker" was originally fitted with a spring and cam unloader which provided a constant lift force independent of the model's vertical position without adding any appreciable mass to the model.

However, after a number of trial runs using the spring and can unloader, examination of the oscillograph tape revealed that

the unloader induced such an extraneous vibration into the system as to make analysis of the acceleration time-history impossible. Therefore, the weight of the model, pole and appendages was unloaded by "negator" type sheave and line constant force springs during the entire range of heave, and downward velocity was imparted by using a ten pound weight on a pan attached to the pole by a "C" clamp. The weight was attached by nylon cord to the fixed (in heave) carriage, Fig. 7, so arranged as to be lifted from the pan at a fixed point before the model hit the water. See Fig. 8. Thusly the model was given downward momentum by the weight and when the weight was lifted off the pan by the cording, the model, being unloaded to a zero "g" condition by the "negator" springs, continued downward at a constant velocity until it struck the water. Examination of subsequent oscillograph tapes revealed that this system, although hurridly improvised due to the limited tank time available, did indeed impart a constant vertical velocity after the weight was lifted off and no discernible vibration to the accelerometer.

The seaplane tank, Tank 3, where the tests were conducted is 313 feet long, 12 feet wide and 6 feet deep when the water level is just even with the opening in the standpipe inside the tank. A maximum carriage speed of 50 feet per second can be attained with the selected speed, amplidyne controlled, carriage driving motor. A tachometer generator, the armature of which is driven by the carriage driving motor shaft, supplies electrical information

to the field of the amplidyne system to provide speed control. With a selected voltage, representing a certain speed, the carriage speed can be maintained to within 0.06 feet per second.

The speed of the towing carriage is measured and recorded by an electronic tachometer specially designed and built by the General Electric Company. The accuracy of this instrument is in the order of a quarter of one percent of the speed being measured, in line with the degree of accuracy required in the drive system.

The instrument receives its impulses for speed measurement from photoelectric scanning discs mounted on the cable-drum shaft. By suitable selection of the number of scanning holes and use of band-spread switches, a small increment of speed can be selected and expanded to cover the full scale of the instrument so as to insure a high degree of accuracy of speed measurement.

As an auxiliary means of determining carriage speed, a mechanical "chronograph" device is used in which the distance travelled by the carriage during measured time intervals is plotted on moving paper tape.

The models were installed in the overhead towing carriage as shown in Figs. 5, 6, 7 and 8 with provisions made to set the angle of trim by a spirit level protractor. With the trim angle set at zero degrees, adjustments were made to insure that there was no angle of roll or yaw. By lowering the model into the water and marking the free surface intersection on either side, roll was considered zero when the wetted length of foil span on either

side of the centerline was equal to the other. Yaw was checked by attaching a straight machined bar with its lengthwise axis in the direction of motion to the model strut. Then, if by moving the carriage forward the edge of the bar remained at a constant distance from the tank wall, yaw was considered zero.

Calibration in heave was made by moving the pole up and down in one inch increments. Heave tape readings were made at each position. Therefore inches of tape per inch of actual heave could be determined.

Calibration in acceleration was made by detaching the accelerometer from the pole and standing it upright (zero "g"), on its side (minus one "g") and upside-down (minus two "g"), and taking tape readings at each position. Thus inches tape per "g" could be determined.

Calibration in heave and acceleration was made daily before starting runs and whenever a change in set-up was made.

In addition, before each run heave was marked on each tape at the bottom stop; where the trailing edge tips of the model just touched the water; and where the trailing edge apex of the model just touched the water. From the intersection of the apex touching trace with the running heave trace, the beginning and end of impact was determined.

Runs were made at a constant forward speed of about 30.7 ft./sec. and for each trim angle, various vertical velocities, see Table III. The vertical velocities in each case could

not be precomputed due to friction in the pole and the stretching of the nylon cord which varied the length of drop over which the weight acted. All vertical velocities were computed from the heave vs. time oscillograph tape.

During the planning phase of these tests it was concluded that in full scale landings full ventilation of the upper foil surface would undoubtedly occur. In order to simulate actual expected conditions, the experiments were planned to achieve separation at the leading edge and consequent ventilation by a combination of high forward speed and a sharp leading edge.

As demonstrated by Wu (Ref. 12) with full ventilation the lift coefficient of a submerged planing flat plate may be predicted by the Rayleigh formula $C_L = \frac{2\pi \sin\tau}{4 + \pi \sin\tau}$, which can be modified for the effect of dihedral on angle of attack to yield $C_L = \frac{2\pi \sin\tau \cos\beta}{4 + \pi \sin\tau \cos\beta}$. After a few trial impact runs it became evident that the modified Rayleigh lift coefficient was not being realized at low trim angles. It was concluded that this was due to the fact that the models, being designed for rigidity and economy of fabrication, had too large a leading edge angle to achieve separation at low trims, and that at trims below the critical separation trim the upper surface was actually generating negative lift. Since funds were not available to reconstruct the models, the trim angle was increased to a minimum of 12° for the tapered-chord foil (Foil #1) and 10° for the constant-chord foil (Foil #2), where positive lift was attained. It was

further concluded separation and subsequent ventilation occurred at and above these trims and they were the minimum examined in the impact condition.

In order to obtain accurate lift data for the impact conditions, planing data was obtained experimentally for both foils at the trim angles and horizontal speed considered in impact. This experimental lift vs. draft data is plotted in Figs. 9 and 10 for Foils 1 and 2, respectively. This planing data was obtained by the same apparatus. After unloading the model and pole with "negator" springs to a zero "g" condition, known weights were attached to the model and it was run down the tank at the forward speed to be examined in impact in a free-to-heave condition. When the predetermined steady speed was reached, the heave (model draft) was read from the visual scale of the oscillograph. The plots of lift vs. draft were obtained by varying the load.

COMPARISON OF THEORETICAL RESULTS WITH EXPERIMENTAL DATA

General Discussion In order to determine the applicability and degree of accuracy of the developed impact theory to the specific case of the dihedral hydrofoil, a comparison was made with experimental model test data. The results of the tests are presented as: (1) experimental curves of vertical steady-state planing force vs. draft, Figs. 9 and 10 for foils 1 and 2 respectively, made at the single horizontal velocity and at the various

trim angles examined in impact. The trim angles used were high enough to insure ventilation in the planing condition; (2) curves of the function $\int_0^z F_z \, dz$ vs. draft obtained from graphical integration of the lift/draft curves. These curves are presented as Figs. 11 and 12 for foils 1 and 2 respectively; (3) plots of maximum loading per run vs. initial flight-path angle, Figs. 13 and 14 for foils 1 and 2 respectively; (4) time-history comparisons with results obtained from the stepwise integration of the equation of motion, equation (18). See Figs. 15 through 32; and (5) loop curves to compare energy absorbing efficiency of the two models at one initial condition, see Fig. 33.

Experimental Data The experimental data obtained in the tests were: (1) curves of steady-state planing force vs. draft necessary in the computation of the theoretical time-histories and (2) experimental time-histories of draft and vertical acceleration. Experimental draft and acceleration were measured directly from the oscillograph tape. The initial vertical velocity, measurement of which is extremely important for an accurate comparison between theory and experiment, was computed from the slope of the draft trace just before water contact. Correct interpretation of the slope of the draft trace is quite dependent upon the judgment of the observer. For this reason, the initial vertical velocities were computed independently by both investigators and the reconciled values were used in this report.

Comparison with Theory Time-histories of experimental draft and acceleration for 18 of the runs listed in Table III are compared in Figs. 15 through 32 with those computed from equation (18) for the same initial conditions. The runs compared were chosen at random and are considered representative of the three trims used and approximately cover the range of initial flight-path angle, γ_o, used in the tests. Again, it is emphasized that full ventilation is expected in full scale landings and that the test impact data is for the case of upper surface ventilation.

Results and Discussion

Acceleration Examination of Figs. 15 through 32 reveals that the presented theory is in excellent agreement with the experimental values of maximum acceleration. However, a general tendency of the experimental time-to-peak to lag the computed is apparent. Although this lag could be blamed on the difficulty in establishing an accurate reference line for acceleration measurement, it is felt that this time lag is a manifestitation of the inherent weakness of the planing analogy, i.e., the treatment of impact as a quasi-static phenomenon. It is well known that pressures on submerged objects as determined by the generalized Bernoulli equation:

$$\frac{V^2}{2} - \frac{\partial \phi}{\partial t} + g\,z + \frac{p}{\rho} = F(t)$$

contain a $\frac{\partial \phi}{\partial t}$ term which increases in importance with increasing

rapidity of time change. For example, in the two-dimensional wedge impact treated by "expanding plate theory" of von Karman and Wagner, the major part of the force results from the $\frac{\partial \phi}{\partial t}$ term. However, this theory, as most potential impact theories, treats the particular case of uniform penetration velocity in which case the $\frac{\partial \phi}{\partial t}$ term furnishes the major resisting force. In decelerated penetration, as in a seaplane landing, the $\frac{\partial \phi}{\partial t}$ term would be reduced by the inertia of the decelerating virtual water mass. In the case considered in the present report, the consideration of impact as quasi-static can be considered as having provided a satisfactory first order answer. With increasing impact velocity however, the effect of the $\frac{\partial \phi}{\partial t}$ term as affected by deceleration can be expected to become more and more important, manifesting itself in a lag of the resisting force. As penetration velocity is reduced and approaches zero the conditions approach static planing and satisfactory agreement of maximum acceleration is expected and in fact obtained.

It is felt a more precise and rigorous impact theory for ventilated hydrofoils can be obtained from potential flow theory. Green's paper, Ref. 13, provides potential equations for the discontinuous flow about a flat plate as does the work of Rayleigh, Ref. 14, and Milne-Thomson, Ref. 15. However, all of these references express the potential function in terms of an intermediate mapping plane and the mathematical difficulties in expressing the potential in terms of the physical plane precluded

further examination of this approach in the time available. It is felt that further examination of the application of the time dependent potential flow theory to hydrofoil impact will be most fruitful.

Draft Comparison of the computed and experimental draft curves of Figs. 15 through 32, show good agreement during initial penetration. However, all experimental values of maximum draft are larger than those computed. It is felt that part of the reason for this deeper penetration is due to the time-lag effects discussed above. Due to the time-lag, the energy is absorbed more slowly than predicted, resulting in a deeper penetration.

Another reason for the variation is considered to be due to separation and ventilation effects. As the vertical velocity becomes small near maximum draft, the flow tends to close over the upper surface of the foil, and for these particular foils this reduces the lift. With less lift to resist penetration, the draft is increased.

The ventilation effects are especially evident at low trim angles. For foil 1 at 12° trim and for foil 2 at 10° trim, Figs. 15 through 17 and Figs. 24 through 26 respectively show experimental draft values diverging from the computed after maximum draft, while at higher trims the experimental curves generally parallel the computed after maximum draft. Since loss of proper ventilation is more critical at the lower trims, the

divergence of the experimental draft from the computed low trim indicates definite closing in of the flow at low trim and probable closing in effects at the higher trims.

It is felt that these pronounced ventilation effects are due in a large part to the poor hydrodynamic design of the model foils tested. The authors of this work have proposed tests of a dihedral hydrofoil constructed for a dynamic model of an actual aircraft to the Experimental Towing Tank, and the results obtained therefrom should be in much better agreement with theory.

Variation of Maximum Loading with Initial Flight-Path Angle

Figs. 13 and 14 reveal that the maximum loading of a dihedral hydrofoil increases linearly with initial flight-path angle, and with a slight increase of maximum loading with increasing trim.

Effect of the Virtual Mass Term $\left(\frac{1}{1+\mu'}\right)$ of Equation (18)

Analysis of ten hand calculated step-by-step integrations of the equation of motion, of which Table I is a sample, reveals that the $\frac{1}{1+\mu'}$ term of equation (18) is conservative, with a minimum observed value at maximum loading of .90 . Therefore its omission in initial estimate of maximum loading, which greatly simplifies hand calculation, should result in a maximum overestimate of maximum loading of approximately 10%.

Usefulness of Sample Computer Program of Table II Comparison of results obtained from the digital computer program of Table II with hand calculated results revealed the use of the computer

resulted in a much greater degree of accuracy than possible with a slide rule at a great saving in time. Calculation of the complete time-history of impact by hand took approximately two hours. Calculation by the digital computer took about 3 minutes of computer running time.

Possible Application Although the hydrofoil models of these tests were designed primarily for verification of the use of planing data to compute hydrofoil impact loads, the general configuration of the models is envisioned as being suitable for seaplane installation. To afford some first-order degree of approximation as to the advantages of such a hydrofoil system, consider the models to be scaled up by a factor of 11.9. This corresponds to an aircraft having a landing speed of 63 knots and a gross weight of 9050 lbs. for foil 1 and 8000 lbs. for foil 2. Since these weights and speed are comparable to the Grumman JRF, the 5 foot beam and 30° deadrise angle of the JRF were selected as further comparison parameters. Using Milwitsky's tables for chines-dry impact, Ref. 16, and the 10.3° flight-path angle of runs 1 and 37 for foils 1 and 2 respectively, maximum load factors for the chines-dry hull impact were computed as 7.3"g" and 7.6"g" respectively. Comparison of these predicted loads with the hydrofoil loads as listed in Table III for the same initial conditions show that foil 1 provides a 45% and foil 2 a 56% reduction in maximum impact load over the chines-dry

hull. This reduction is accomplished by a full scale foil of 8.5 ft. span and the following chord dimensions:

For foil 1 - an apex chord of 11.9 inches and a tip chord of 23.8 inches.

For foil 2 - a constant chord of 11.9 inches.

To consider the foils as energy absorbing devices, the loop charts of Fig. 33 were constructed. Graphically integrating the area under the curves to the point of maximum penetration checked the initial kinetic energy, $\frac{1}{2} M \dot{z}_o^2$, within 5%. Furthermore, comparing the area under the curves with the square area of an ideal shock absorber showed both foils to have an ideal efficiency of approximately 56%. However, taking the ratio of rebound energy (area under lower limb of loop curve) to input energy (area under upper limb), showed that foil 1 returned only 17.5% of the original kinetic energy to the system as rebound while foil 2 returned 28.4%. Therefore, a tapered foil corresponding to the dimensions of foil 1 would provide a more damped landing device with lesser likelihood of the heavy damage experienced with the rebound impacts of the conventional hull.

Conclusions An analysis of the experimental data obtained during hydrodynamic impact of a dihedral hydrofoil resulted in the following conclusions:

(1) In general, the use of the quasi-static planing analogy to compute hydrofoil impact loads gives a good all-around approach.

In particular, computed maximum loadings are in very good agreement with experiment, showing an average error of 6.2% for 47 runs.

(2) Experimental time-to-peak tends to lag the computed.

(3) Correspondence between computed and experimental draft is good until maximum force, after which a divergence is noted due to the time-lag of (2) above and separation effects.

(4) The maximum impact loading of a dihedral hydrofoil increases linearly with initial flight-path angle and increases slightly with increasing trim.

(5) The effect of the Virtual Mass Term $\left(\frac{1}{1+\mu'}\right)$ of equation (18) is conservative, with a minimum observed value at maximum loading of .90.

(6) The sample digital computer program of Table II improves the accuracy of the calculation of draft and acceleration time-histories and reduces the time required for such calculation from 2 hours to 3 minutes.

(7) Compared with chines-dry impact at a 10.3° flight-path angle, the dihedral hydrofoil system offers a reduction of maximum impact loading in the order of 50%.

(8) At approximately 8.9° initial flight-path angle, both foils tested had an ideal shock absorber efficiency of 56%; however the larger tapered foil 1 returned but 17.5% of the original kinetic energy to the system as rebound energy, while foil 2 returned 28.4%, and therefore a foil similar to foil 1 is recommended for its damping qualities.

BIBLIOGRAPHY

1. von Karman, Th. The Impact of Seaplane Floats during Landing. NACA TN No. 321, 1929.

2. Wagner, Herbert. Landing of Seaplanes. NACA TM No. 622, 1931.

3. Pabst, Wilhelm. Theory of the Landing Impact of Seaplanes. NACA TM No. 580, 1930.

4. Mayo, Wilbur. Analysis and Modification of Theory for Impact of Seaplanes on Water. NACA TN No. 1008, 1945.

5. Steiner, Margaret. Analysis of Planing Data for Use in Predicting Hydrodynamic Impact Loads. NACA TN No. 1694, 1948.

6. Smiley, Robert F. An Experimental Study of Water Pressure Distributions During Landing and Planing of a Heavily Loaded Flat-Plate Model. NACA TN No. 2453, 1951.

7. Schnitzer, Emanuel. Theory and Procedure for Determining Loads and Motions in Chine-Immersed Hydrodynamic Impacts of Prismatic Bodies. NACA TN No. 2813, 1952.

8. Smiley, Robert F. The Application of Planing Characteristics to the Calculation of the Water Landing Loads and Motions of Seaplanes of Arbitrary Constant Cross Section. NACA TN No. 2814, 1952.

9. Brown, P. Ward. Seaplane Impact Theory. Short's Hydrodynamics Note No. 46, 1954. (Short Brothers and Harland Ltd., Belfast).

10. Monaghan, R.J. A Review of the Essentials of Impact Force Theories for Seaplanes and Suggestions for Approximate Design Formulae. British A.R.C. Report R & M 2720, 1952.

11. Miller, Robert W. Water Landing Investigation of a Flat Bottom V-Step Model and a Comparison with a Theory Incorporating Planing Data. NACA TN No. 2932, 1953.

12. Wu, T. Yao-tsu and Perry, Byrne. Comparison of Characteristics of a Hydrofoil Under Cavitating and Non-Cavitating Operation. California Institute of Technology Report No. 47-4, 1947.

13. Green, A.E. The Gliding of a Plate on a Stream of Finite Depth. Proceedings of the Cambridge Philosophical Society, Vol. 32, 1936.

14. Rayleigh, Lord. On the Resistance of Fluids. Papers, i. 287.

15. Milne-Thomson, L.M. Theoretical Hydrodynamics. London, Macmillan and Co., 1938.

16. Milwitzky, B. A Generalized Theoretical and Experimental Investigation of the Motions and Hydrodynamic Loads Experienced by V-Bottom Seaplanes During Step-Landing Impacts. NACA TN No. 1516, 1948.

TABLE I

Step-by-Step Integration of Equation of Motion - $\ddot{z} = F_z \left[\frac{V_H \sin\tau + \dot{z}\cos\tau}{V_H \sin\tau}\right]^2 \frac{1}{1+\kappa'}$

Run 47, Foil 2 $V_H = 30.66$ fps $\Delta_o = 4.75$ lbs.
$\dot{z}_o = 2.98$ fps $\tau = 14^\circ$

Table shows first 14 points only.

Point, n	0	1	2	3	4	5	6	7	8	9	10	11	12	13	14
Δt, sec.	.005	.005	.005	.005	.006	.005	.005	.005	.005	.005	.005	.005	.005	.005	.006
$n\Delta t$, sec.	0	.005	.010	.015	.020	.025	.030	.035	.040	.045	.050	.055	.060	.065	.070
V_H, fps	30.66	30.66	30.66	30.66	30.86	30.66	30.66	30.66	30.66	30.66	30.66	30.66	30.66	30.66	30.66
$\dot{z}_n$ fps	2.98	2.944	2.837	2.866	2.441	2.176	1.879	1.570	1.255	.942	.639	.346	.070	-.189	-.429
$d_{increment} = \dot{z}_{n-1}\Delta t$, ft.	0	.01490	.01482	.01419	.01333	.01220	.01088	.00940	.00785	.00628	.00471	.00320	.00173	.00035	-.00094
$d_{av\ increment} = \frac{\dot{z}_n \Delta t}{2}$, ft.	0	.00746	.00736	.00710	.00667	.00610	.00544	.00470	.00392	.00314	.00235	.00160	.00086	.00017	-.00047
$d_n = d_{l\,n-1} + \frac{\dot{z}_n \Delta t}{2}$, ft.	0	.00745	.02218	.03638	.04912	.06192	.07279	.08218	.09003	.09641	.10112	.10432	.10604	.10641	.10547
F_z, lbs.	0	.551	1.64	2.69	3.68	4.58	5.38	6.08	6.65	7.12	7.49	7.725	7.85	7.87	7.80
$\int_o^z F_z dz$, ft.-lbs.	0	.001	.02	.05	.09	.15	.195	.25	.30	.343	.372	.40	.42	.421	.41
$V_H \sin\tau$	7.43	7.43	7.43	7.43	7.43	7.43	7.43	7.43	7.43	7.43	7.43	7.43	7.43	7.43	7.43
$\dot{z}\cos\tau$	0	2.89	2.86	2.75	2.59	2.37	2.11	1.82	1.52	1.22	.91	.62	.34	.07	-.18
$V_H \sin\tau + \dot{z}\cos\tau$	7.43	10.32	10.29	10.18	10.02	9.80	9.54	9.25	8.95	8.65	8.34	8.05	7.77	7.50	7.25
$\frac{V_H \sin\tau + \dot{z}\cos\tau}{V_H \sin\tau}$	1	1.39	1.386	1.37	1.35	1.32	1.283	1.24	1.204	1.164	1.12	1.083	1.045	1.010	.977
$\left[\frac{V_H \sin\tau + \dot{z}\cos\tau}{V_H \sin\tau}\right]^2$	1	1.93	1.92	1.88	1.824	1.74	1.67	1.55	1.45	1.355	1.26	1.175	1.092	1.020	.953
$\kappa' = \frac{g}{\Delta_o V_H^2 \sin^2\tau} \int_o^z F_z dz$	0	.0001	.00246	.0062	.011	.0184	.024	.031	.0368	.042	.0455	.049	.0515	.051	.0507
$\frac{1}{1+\kappa'}$	1	1	.998	.995	.989	.984	.978	.97	.965	.960	.955	.953	.950	.950	.950
$\Delta_i = F_z \left[\frac{V_H \sin\tau + \dot{z}\cos\tau}{V_H \sin\tau}\right]^2 \frac{1}{1+\kappa'}$	0	1.063	3.13	5.03	6.63	7.83	8.75	9.13	9.30	9.24	9.01	8.65	8.16	7.64	7.07
$\ddot{z}/g = \frac{\Delta i}{\Delta_o}$	0	.224	.663	1.06	1.396	1.65	1.842	1.922	1.950	1.945	1.896	1.822	1.718	1.608	1.49
$\dot{z}_n = \dot{z}_{n-1} - \frac{\ddot{z}}{g} g \Delta t$	2.98	2.944	2.837	2.666	2.441	2.176	1.879	1.570	1.255	.942	.639	.346	.070	-.189	-.429
$d_{l\,n} = d_{l\,n-1} + \frac{\dot{z}_n + \dot{z}_{n-1}}{2} \Delta t$	0	.01482	.02928	.04305	.05582	.06735	.07748	.08611	.09327	.09877	.10272	.10518	.10624	.10594	.10440

TABLE II

Part A

Sample Flow Chart for Step-by-Step Computation of Equation of Motion by use of a Digital Computer

* Subroutine Shown is for Foil 2 at $\tau = 12^{\circ}$

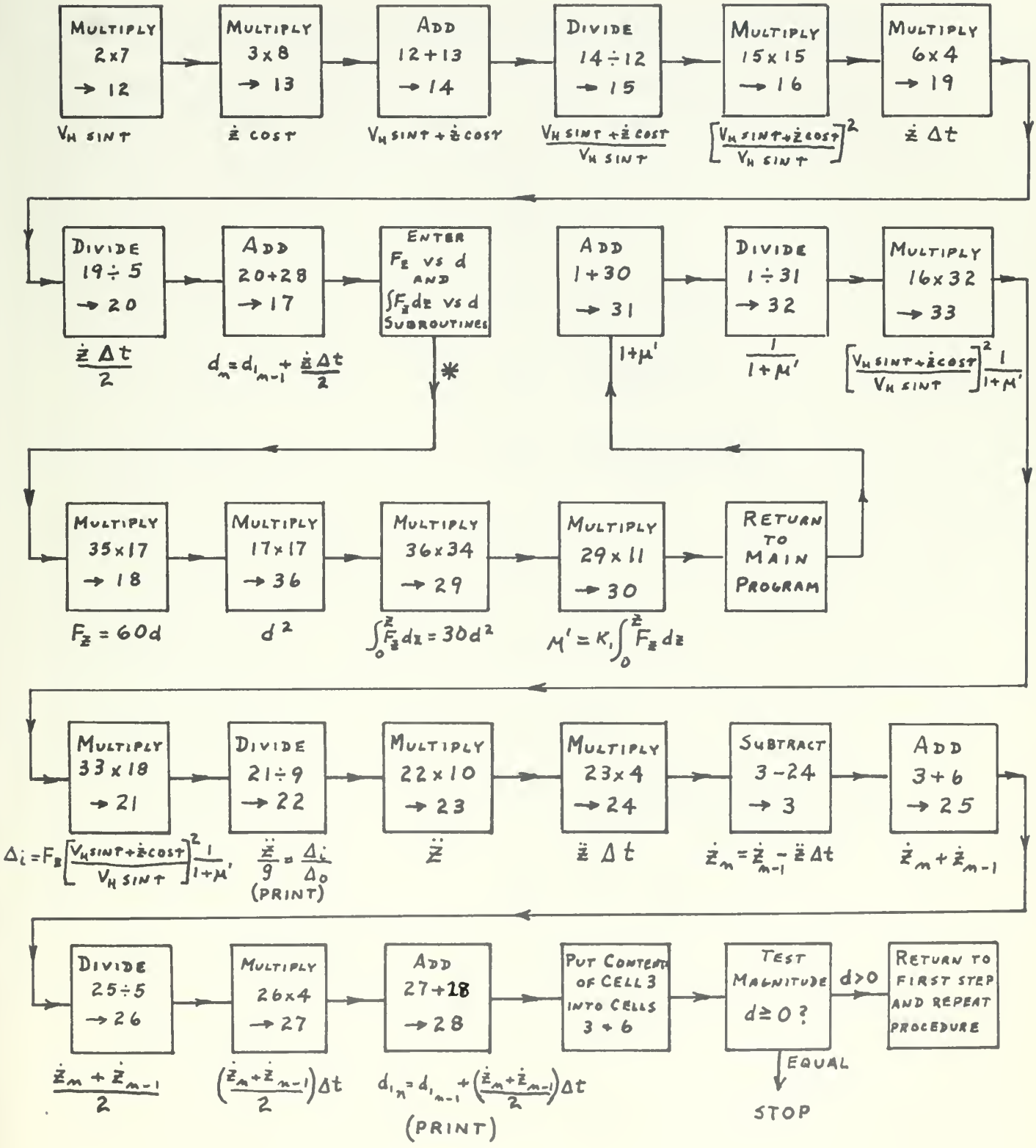

TABLE II

Part B

Cell Fill and Working Storage for Sample Digital Computer Program to Determine Time History of Impact

* Main Program Fill ** Subroutine Fill

\# Main Program Working Storage ## Subroutine Working Storage

Cell	Quantity	Cell	Quantity
1*	1	13#	$\dot{z}\cos\tau$
2*	V_H	14#	$V_H\sin\tau + \dot{z}\cos\tau$
3*	$\dot{z}$	15#	$\frac{V_H\sin\tau + \dot{z}\cos\tau}{V_H\sin\tau}$
4*	Δt	16#	$\left[\frac{V_H\sin\tau + \dot{z}\cos\tau}{V_H\sin\tau}\right]^2$
5*	2	17#	d
6*	$\dot{z}$	18#	F_z
7*	$\sin\tau$	19#	$\dot{z}\,\Delta t$
8*	$\cos\tau$	20#	$\frac{\dot{z}\,\Delta t}{2}$
9*	Δ_o	21#	$\Delta_i = F_z\left[\frac{V_H\sin\tau + \dot{z}\cos\tau}{V_H\sin\tau}\right]^2 \frac{1}{1+\mu'}$
10*	g	22#	$\ddot{z}/g = \Delta_i/\Delta_o$
11*	$k_1 = \frac{g}{\Delta_o V_H^2 \sin^2\tau}$	23#	$\ddot{z}$
12#	$V_H\sin\tau$	24#	$\ddot{z}\,\Delta t$

TABLE II

Part B (Cont'd.)

Cell	Quantity	Cell	Quantity
25#	$\dot{z}_n + \dot{z}_{n-1}$	31#	$1 + \mu'$
26#	$\frac{\dot{z}_n + \dot{z}_{n-1}}{2}$	32#	$\frac{1}{1 + \mu'}$
27#	$(\frac{\dot{z}_n + \dot{z}_{n-1}}{2})\Delta t$	33#	$\left[\frac{V_H \sin\tau + \dot{z}\cos\tau}{V_H \sin\tau} \right]^2 \frac{1}{1 + \mu'}$
28#	$d_{l_n} = d_{l_{n-1}} (\frac{\dot{z}_n + \dot{z}_{n-1}}{2})\Delta t$	34**	30
29#	$\int_o^z F_z dz$	35**	60
30#	$\mu' = k_1 \int_o^z F_z dz$	36##	d^2

TABLE III

EXPERIMENTAL IMPACT RUNS

V_H = 30.66 fps = Constant

Foil 1

$\tau = 12^\circ$

Run	$\dot{z}_o$ fps	γ_o deg.	g max. comp.	g max. exper.	% error
1	5.52	10.3	3.95	4.00	1.25
2	4.64	8.7	3.13	3.45	9.23
3	3.62	6.7	2.28	2.40	5.00
4	6.15	11.3	4.56	4.50	1.33
5	5.45	10.2	3.88	3.71	4.46
6	4.80	8.9	3.27	3.27	0
7	3.78	7.1	2.40	2.76	13.00
8	2.94	5.5	1.74	1.78	2.24
9	1.76	3.3	.95	1.16	18.10

$\tau = 14^\circ$

10	5.89	11.0	4.81	5.20	7.5
11	5.21	9.8	4.10	4.00	2.5
12	3.40	6.4	2.43	2.75	11.5
13	5.35	9.9	4.23	4.21	.47
14	4.69	8.7	3.60	3.58	.56
15	3.88	7.3	2.85	3.02	5.60
16	2.95	5.5	2.04	2.08	1.92
17	6.22	11.6	5.14	4.80	7.10

$\tau = 15.5^\circ$

18	5.84	10.8	5.03	4.97	1.21
19	5.17	9.6	4.24	4.22	.47
20	4.53	8.4	3.64	3.62	.57
21	3.30	6.1	2.98	2.60	14.60

Foil 2

$\tau = 10^\circ$

Run	$\dot{z}_o$ fps	γ_o deg.	g max. comp.	g max. exper.	% error
22	4.65	8.7	2.48	2.60	4.6
23	1.60	3.0	.75	.70	7.1
24	2.68	5.0	1.29	1.55	16.7
25	3.95	7.4	2.02	2.15	6.0
26	5.00	9.3	2.70	2.75	1.8
27	4.00	7.5	2.03	2.18	6.9
28	2.83	5.3	1.36	1.60	15.0
29	5.15	11.5	2.77	2.75	.7

$\tau = 12^\circ$

30	5.22	9.6	3.44	3.13	9.9
31	4.37	8.1	2.78	2.96	6.1
32	4.17	7.7	2.63	2.55	3.1
33	3.53	6.6	2.18	2.11	3.3
34	2.72	5.1	1.64	1.39	18.0
35	1.22	2.3	.72	.71	1.4
36	5.65	10.4	3.75	3.32	13.0
37	5.57	10.3	3.70	3.32	11.5
38	4.76	8.8	3.03	2.92	3.8
39	3.84	7.1	2.36	2.55	7.5
40	2.87	5.4	1.78	1.84	3.2

$\tau = 14^\circ$

41	5.27	9.7	3.76	3.73	.8
42	4.51	8.4	3.12	3.22	3.1
43	3.98	7.4	2.73	2.91	6.2
44	4.04	7.5	2.76	2.34	18.4
45	5.46	10.1	3.86	3.47	11.2
46	4.10	7.6	2.78	2.73	1.8
47	2.98	5.5	1.95	1.92	1.5

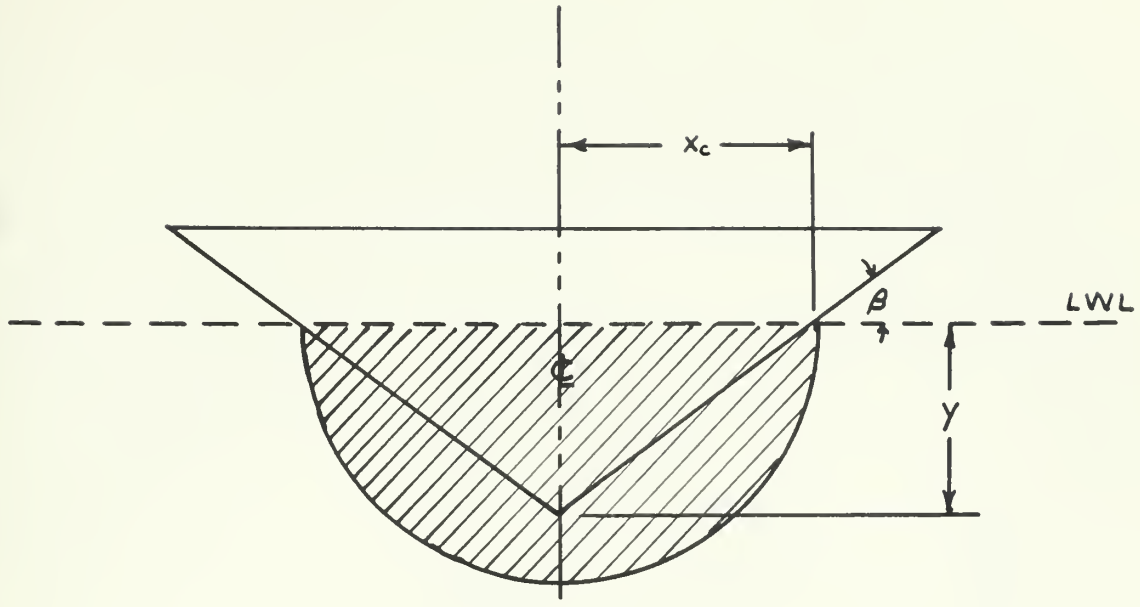

VON KARMAN'S TWO-DIMENSIONAL
VIRTUAL MASS FOR
AN IMPACTING WEDGE

FIG.1

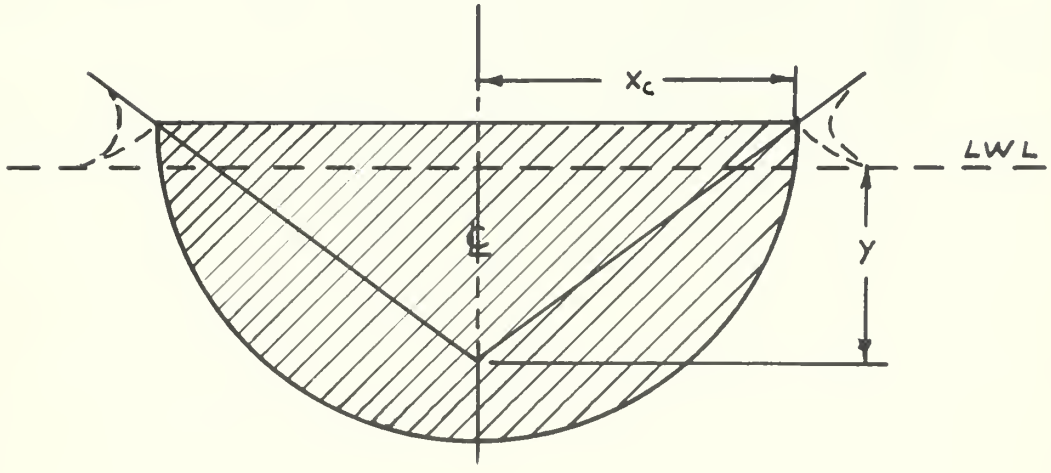

WAGNER'S TWO-DIMENSIONAL
VIRTUAL MASS FOR
AN IMPACTING WEDGE

FIG.1a

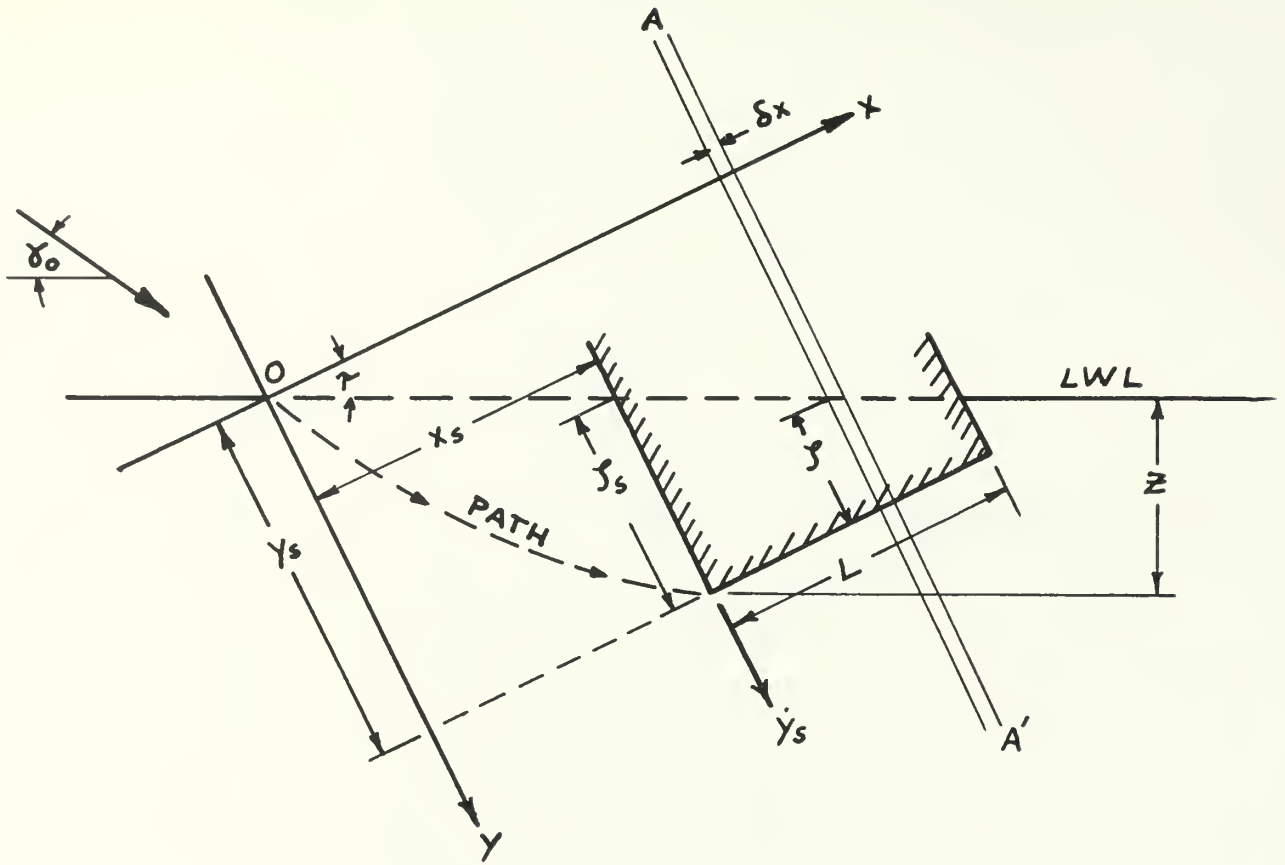

OBLIQUE IMPACT OF AN ARBITRARY BODY

FIG. 2

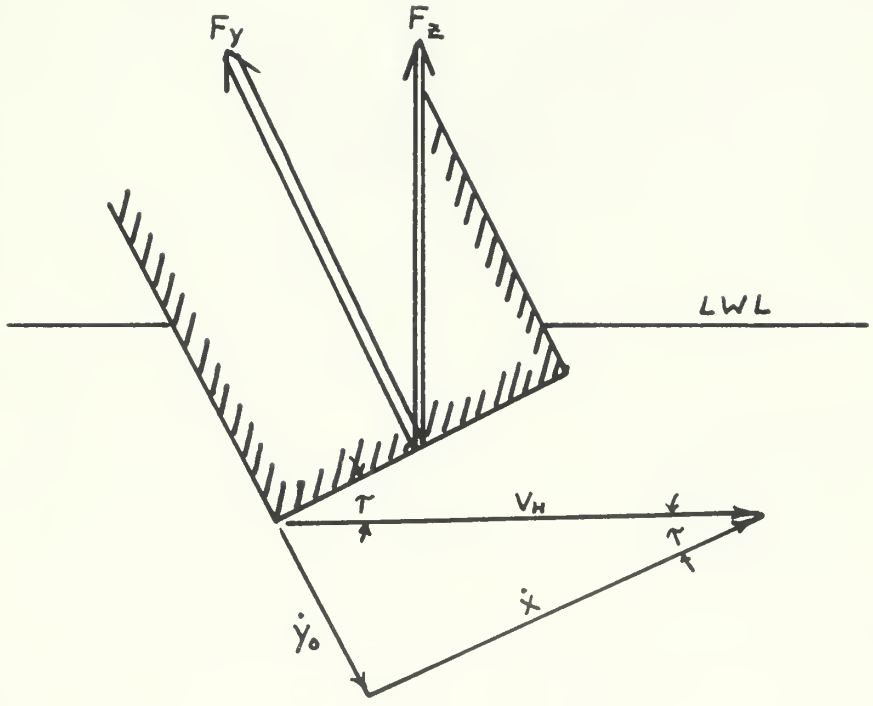

PLANING FORCE DIAGRAM

FIG. 3

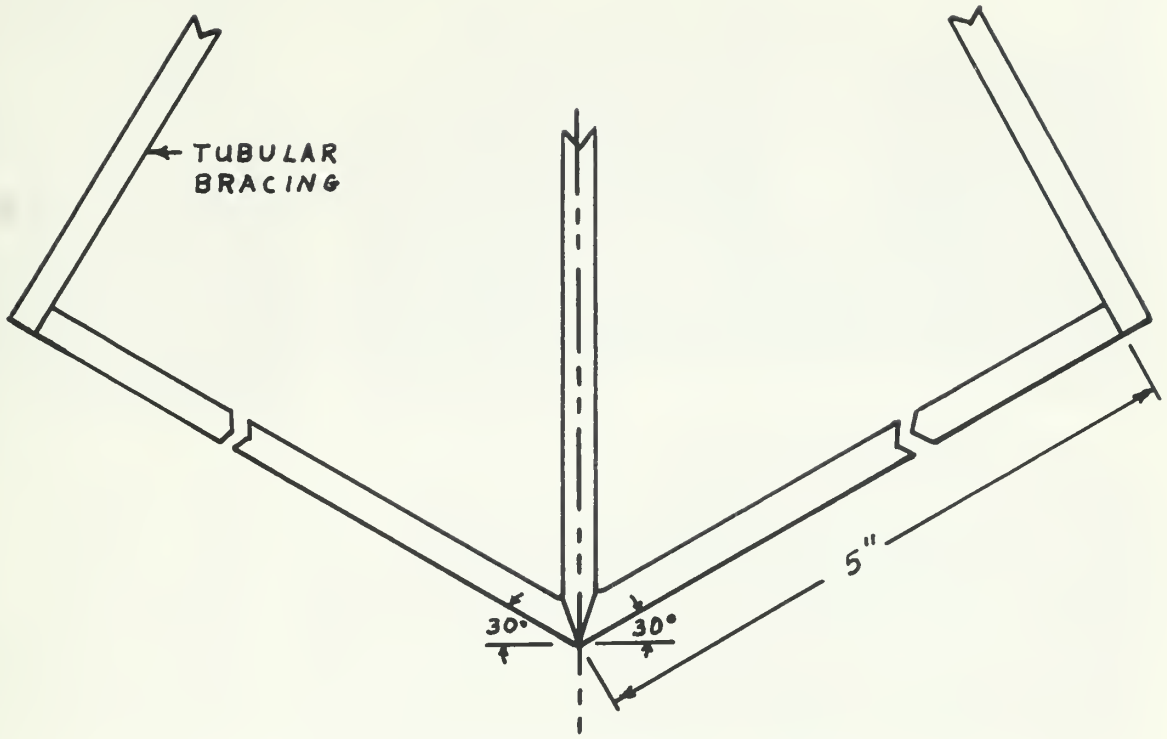

FRONT VIEW

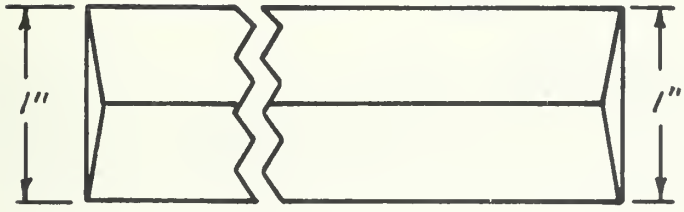

TOP VIEW FOIL#2

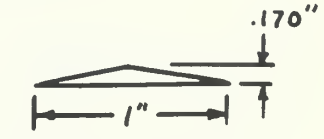

CROSS SECTION FOIL#2

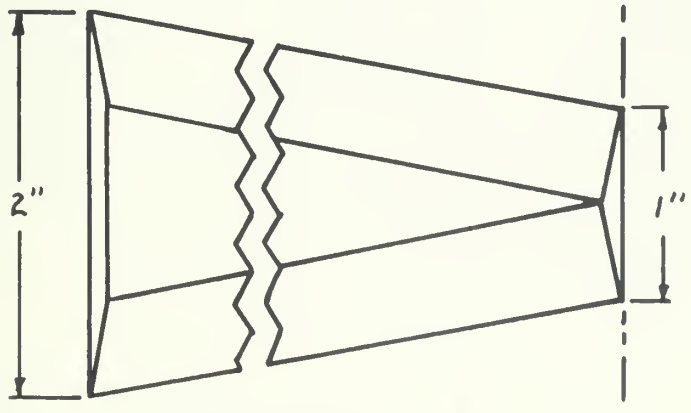

TOP VIEW FOIL#1

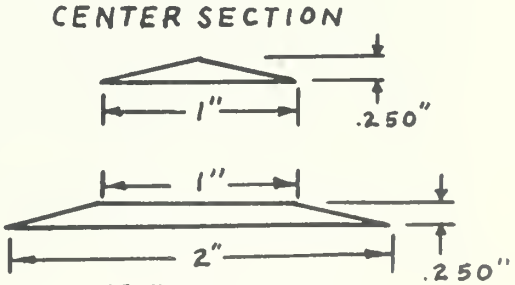

FOIL#1

HYDROFOIL MODELS

FIG. 4

APPARATUS SET-UP WITH FOIL#2
SHOWING THE SPRING-AND-CAM UNLOADER
FIG.5

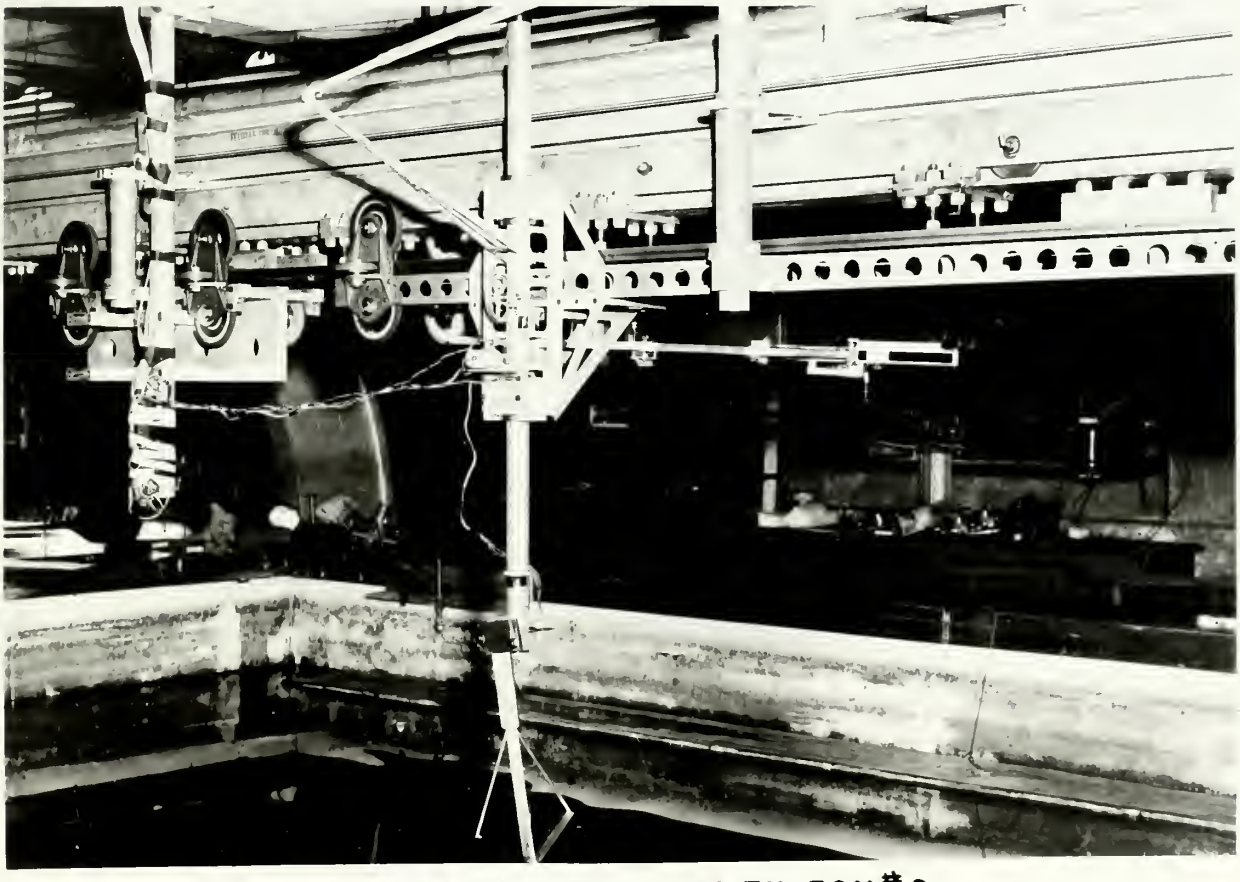

APPARATUS SET-UP WITH FOIL#2
SHOWING THE "NUTCRACKER"
FIG. 6

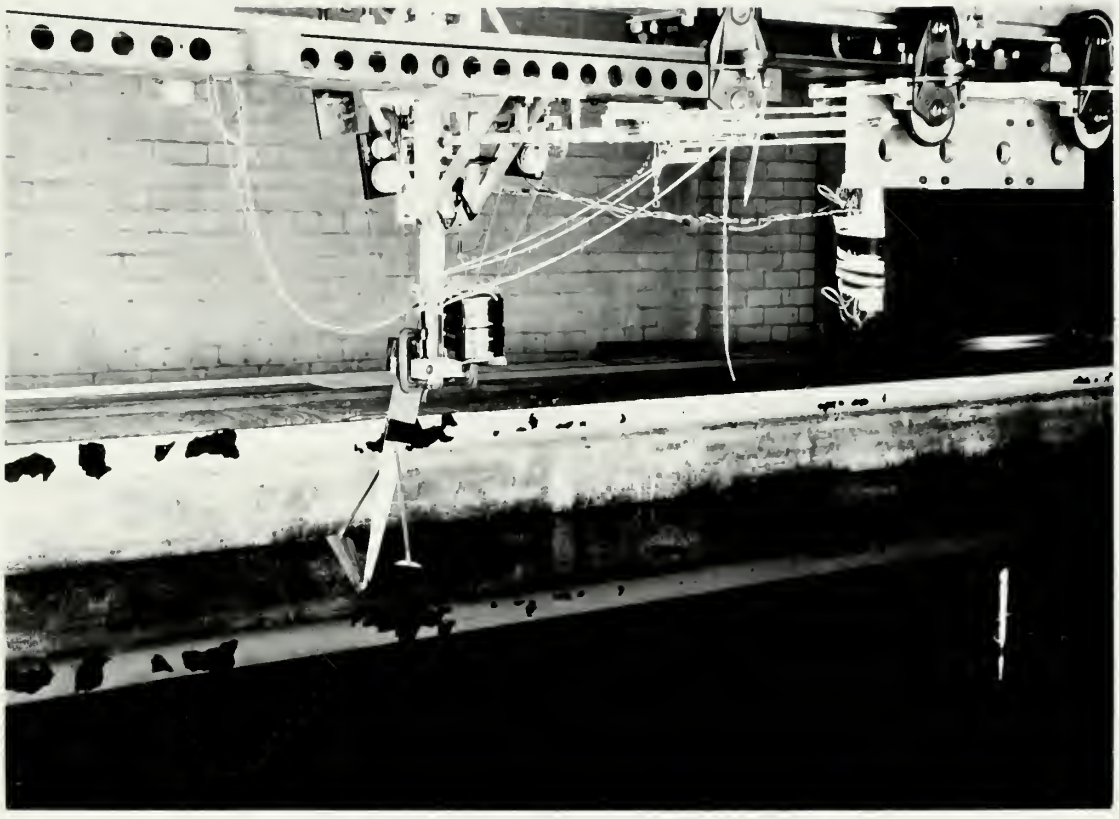

APPARATUS SET-UP WITH FOIL #1
SHOWING MODEL AND TEN POUND WEIGHT
BEFORE RELEASE
FIG. 7

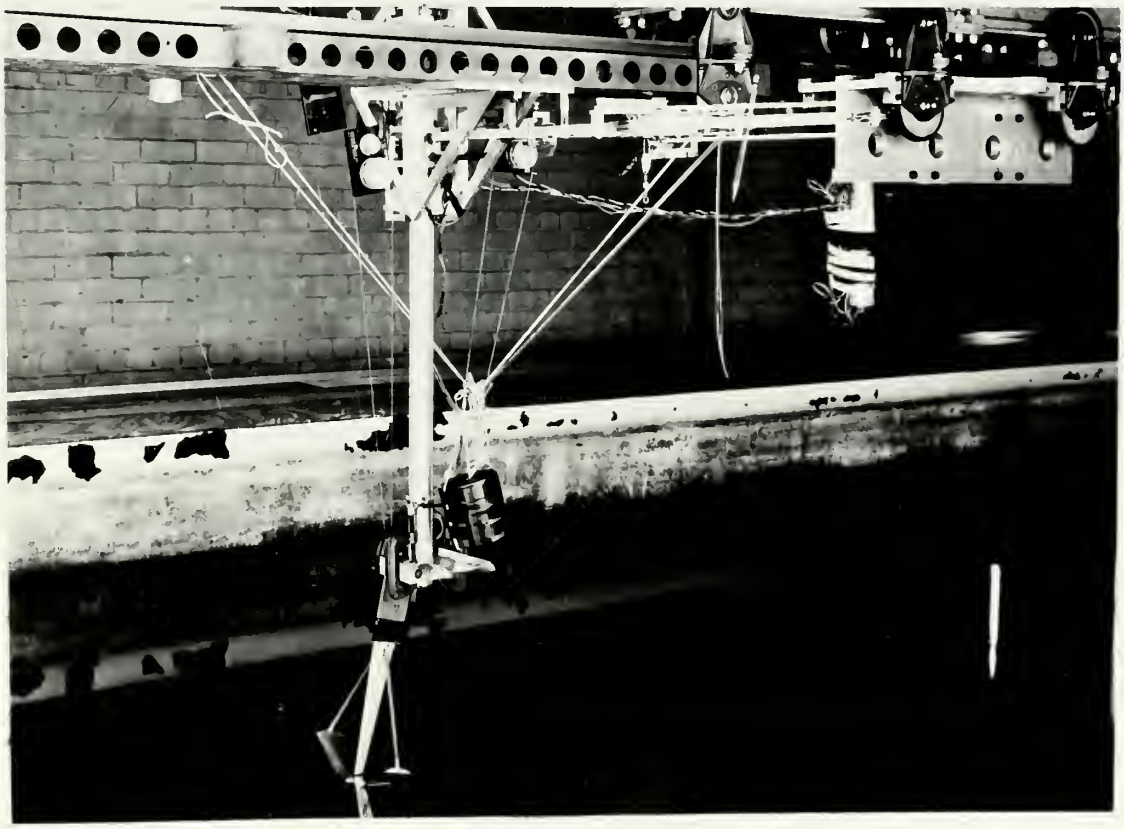

APPARATUS SET-UP WITH FOIL 1
SHOWING MODEL AND TEN POUND WEIGHT
AFTER RELEASE
FIG. 8

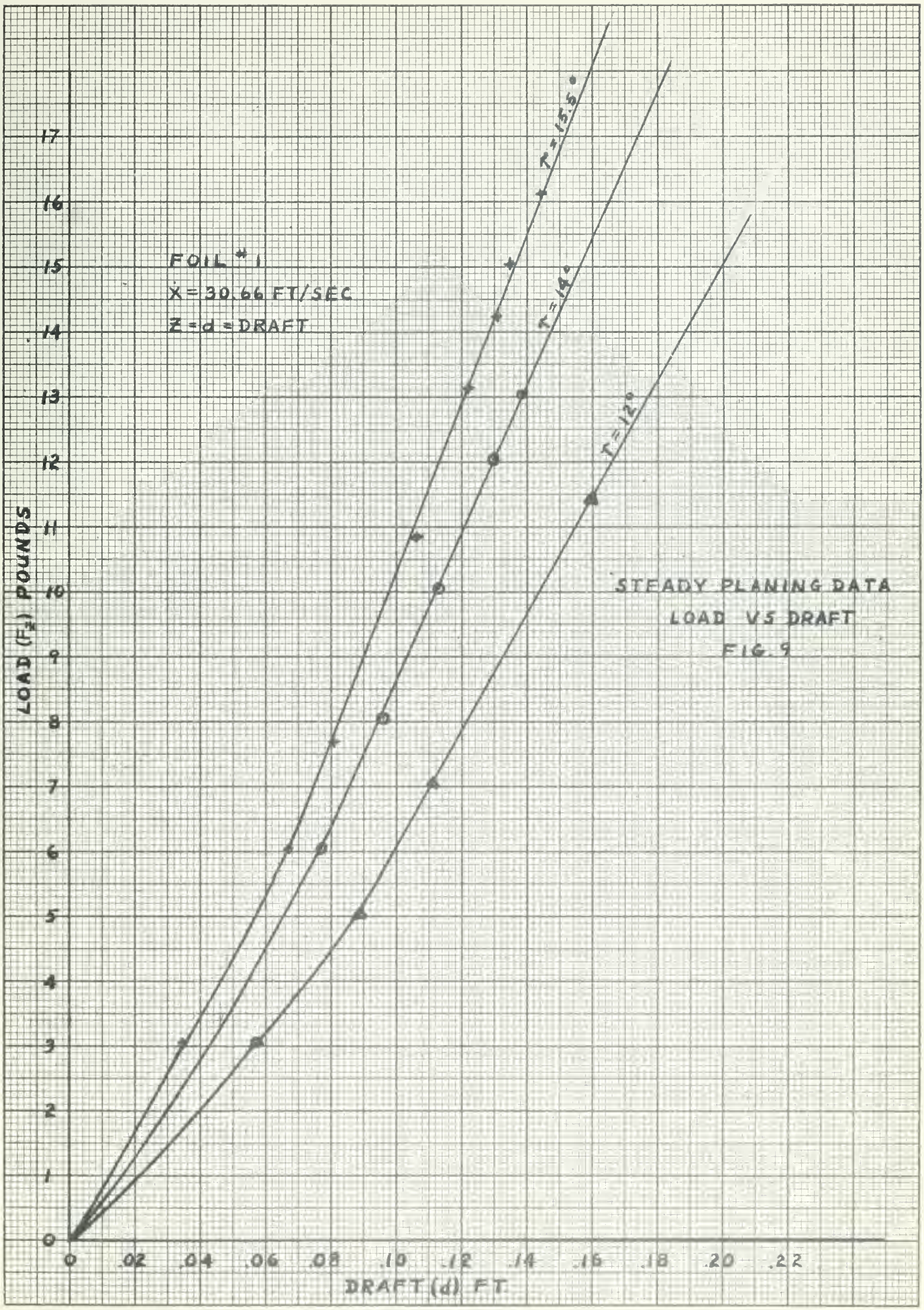

STEADY PLANING DATA
LOAD VS DRAFT
FIG. 9

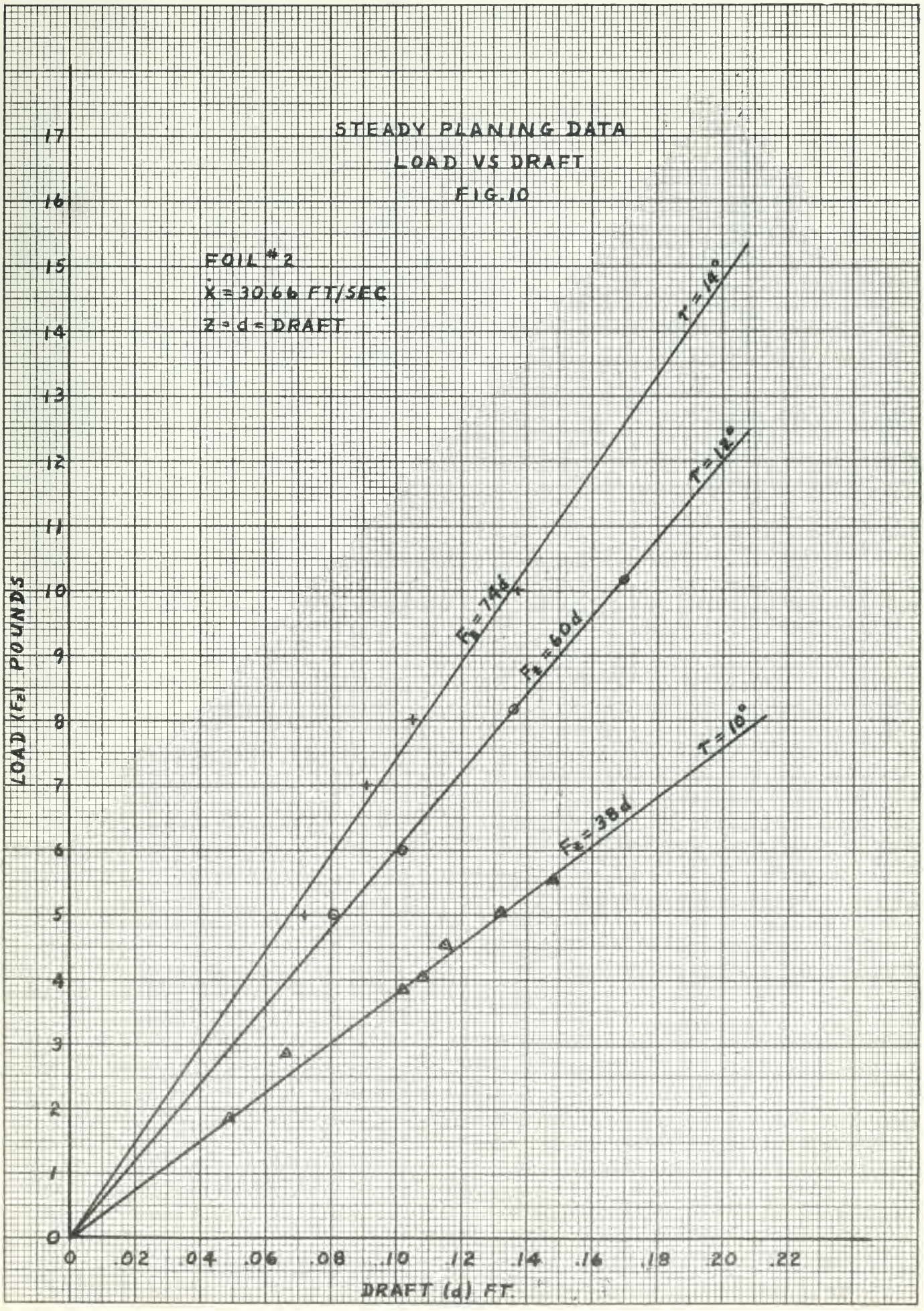
STEADY PLANING DATA
LOAD VS DRAFT
FIG. 10
FOIL # 2
X = 30.66 FT/SEC
Z = d = DRAFT
T = 14°
T = 12°
T = 10°
Fz = 74d
Fz = 60d
Fz = 38d
LOAD (Fz) POUNDS
DRAFT (d) FT.
0
1
2
3
4
5
6
7
8
9
10
11
12
13
14
15
16
17
.02
.04
.06
.08
.10
.12
.14
.16
.18
.20
.22

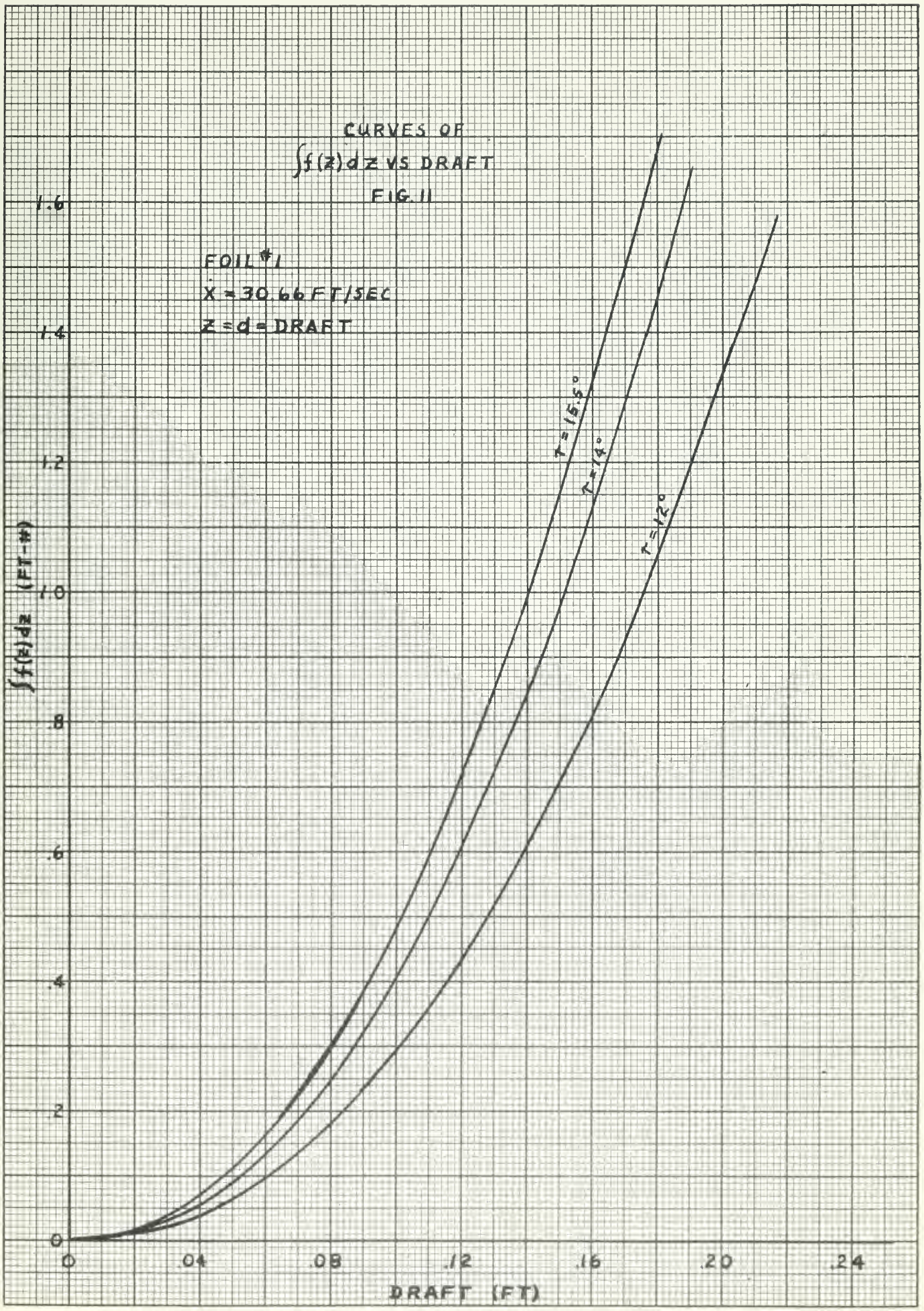
CURVES OF
$\int f(z)dz$ VS DRAFT
FIG. 11
FOIL #1
X = 30.66 FT/SEC
Z = d = DRAFT
τ = 15.5°
τ = 14°
τ = 12°
$\int f(z)dz$ (FT-#)
DRAFT (FT)
0
.2
.4
.6
.8
1.0
1.2
1.4
1.6
0
.04
.08
.12
.16
.20
.24

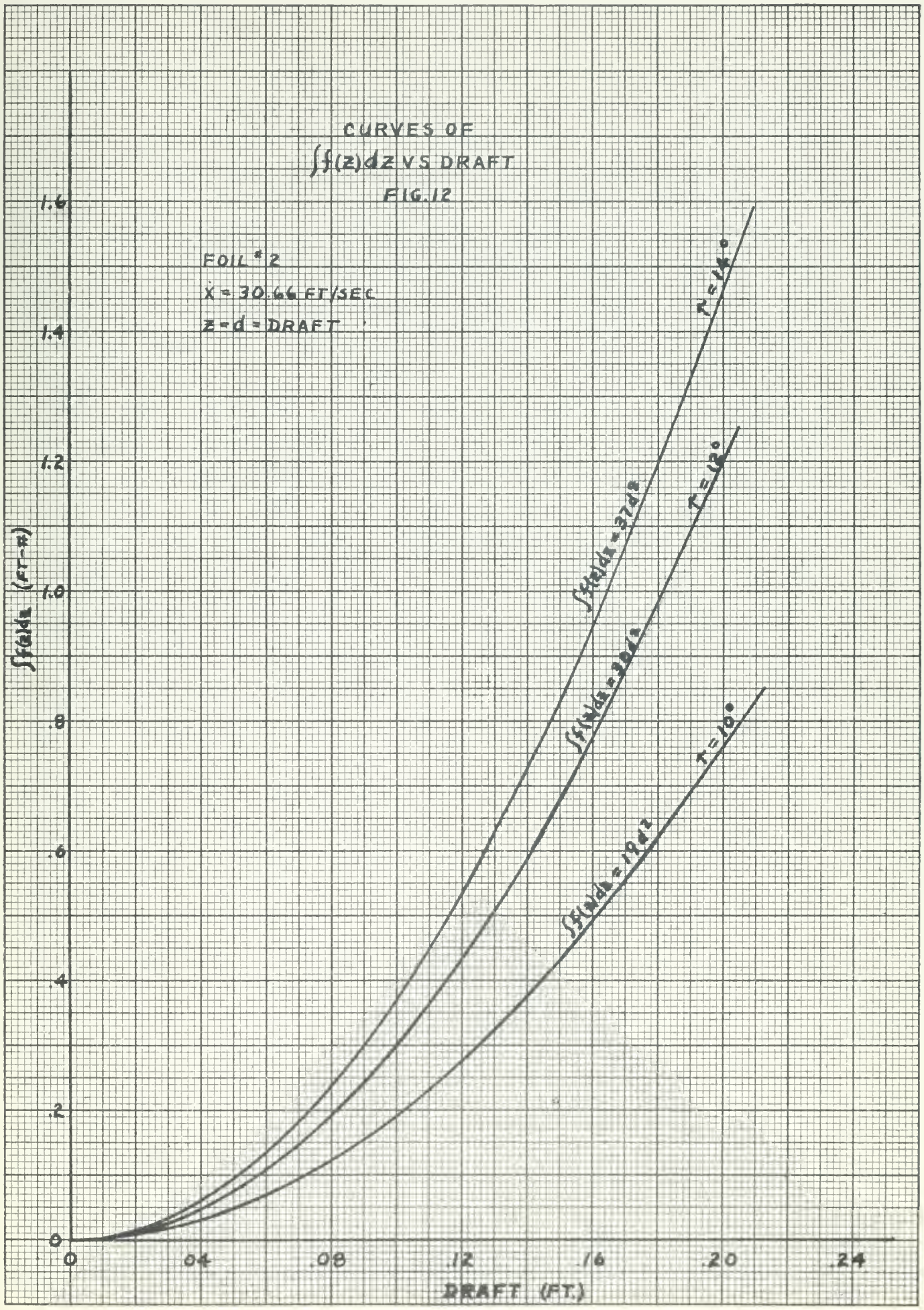
CURVES OF
$\int f(z)dz$ VS DRAFT
FIG. 12
FOIL # 2
X = 30.66 FT/SEC
z = d = DRAFT
$\int f(z)dz$ (FT-#)
1.6
1.4
1.2
1.0
.8
.6
.4
.2
0
$\int f(z)dz = 37d^2$
$\int f(z)dz = 30d^2$
$\int f(z)dz = 19d^2$
T = 14°
T = 12°
T = 10°
0
.04
.08
.12
.16
.20
.24
DRAFT (FT.)

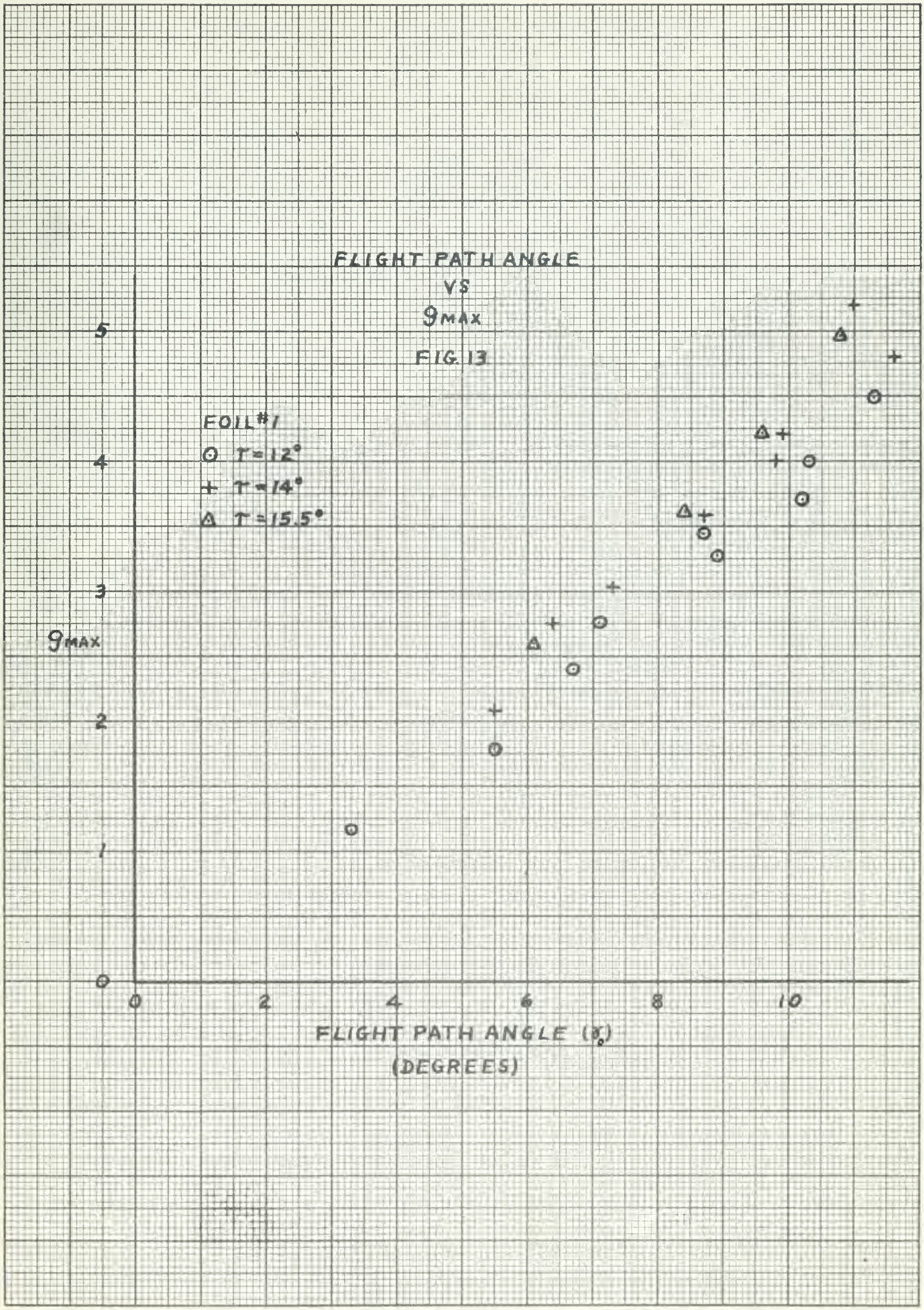
FLIGHT PATH ANGLE
VS
g_{MAX}
FIG. 13
FOIL #1
⊙ τ = 12°
+ τ = 14°
△ τ = 15.5°
g_{MAX}
0
1
2
3
4
5
0
2
4
6
8
10
FLIGHT PATH ANGLE (γ_o)
(DEGREES)

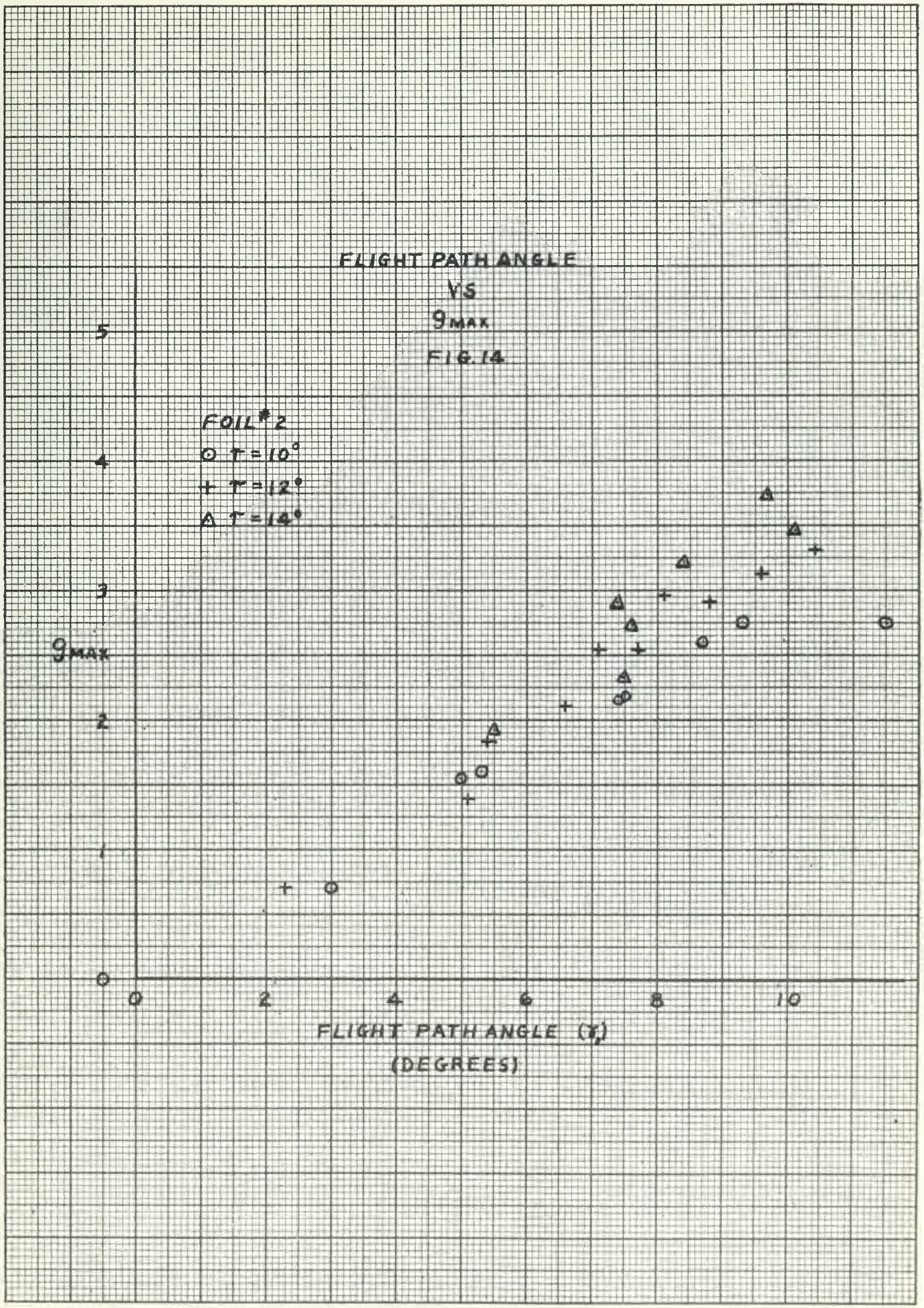
FLIGHT PATH ANGLE
VS
g_{MAX}
FIG. 14
FOIL # 2
⊙ T = 10°
+ T = 12°
△ T = 14°
g_{MAX}
5
4
3
2
1
0
0
2
4
6
8
10
FLIGHT PATH ANGLE (γ_i)
(DEGREES)

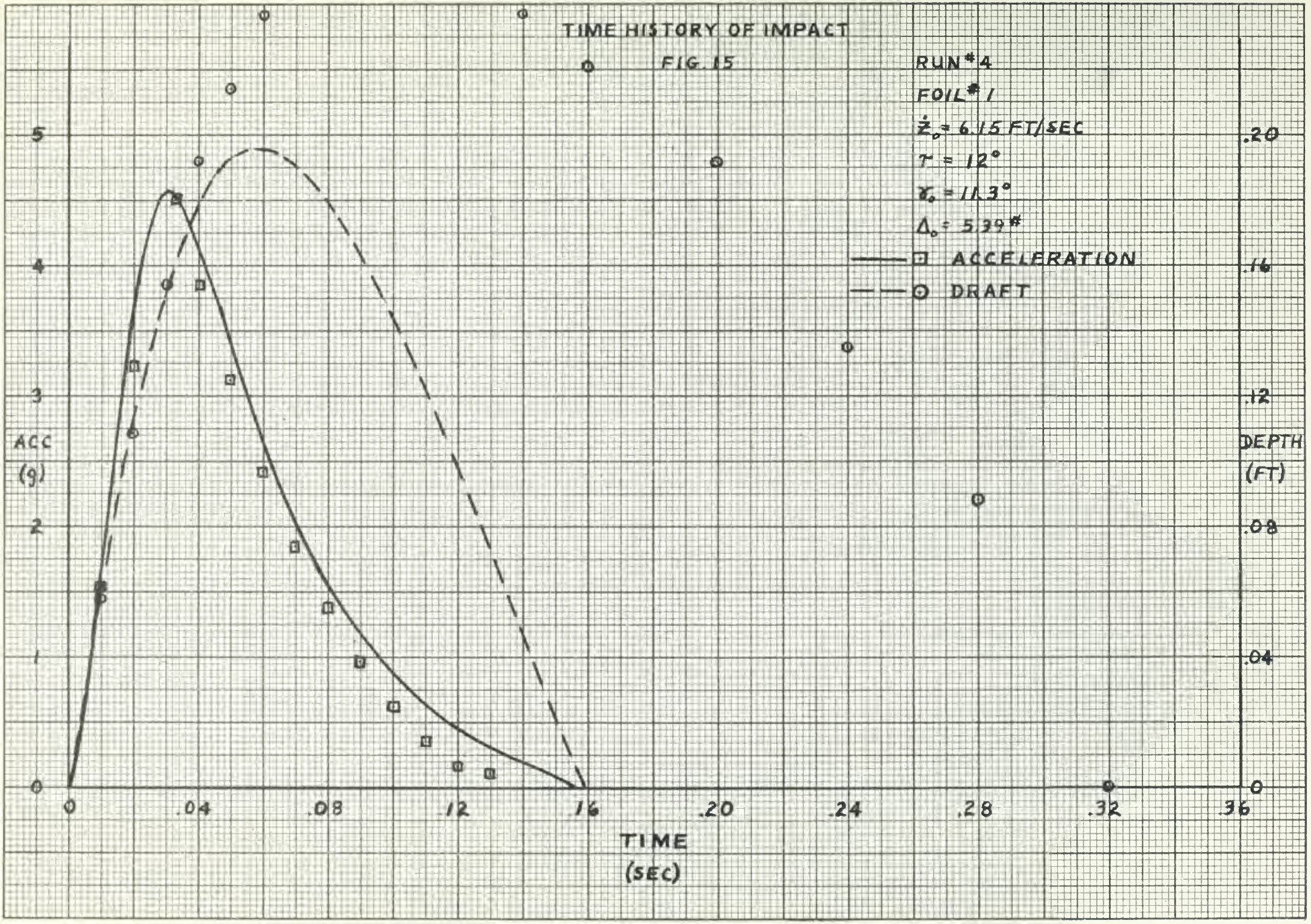
TIME HISTORY OF IMPACT
FIG. 15
RUN # 4
FOIL # 1
$\dot{z}_o$ = 6.15 FT/SEC
τ = 12°
γ_o = 11.3°
Δ_o = 5.39#
ACCELERATION
DRAFT
ACC (g)
DEPTH (FT)
TIME (SEC)
0
1
2
3
4
5
.04
.08
.12
.16
.20
.24
.28
.32
.36
.20
.16
.12
.08
.04
0

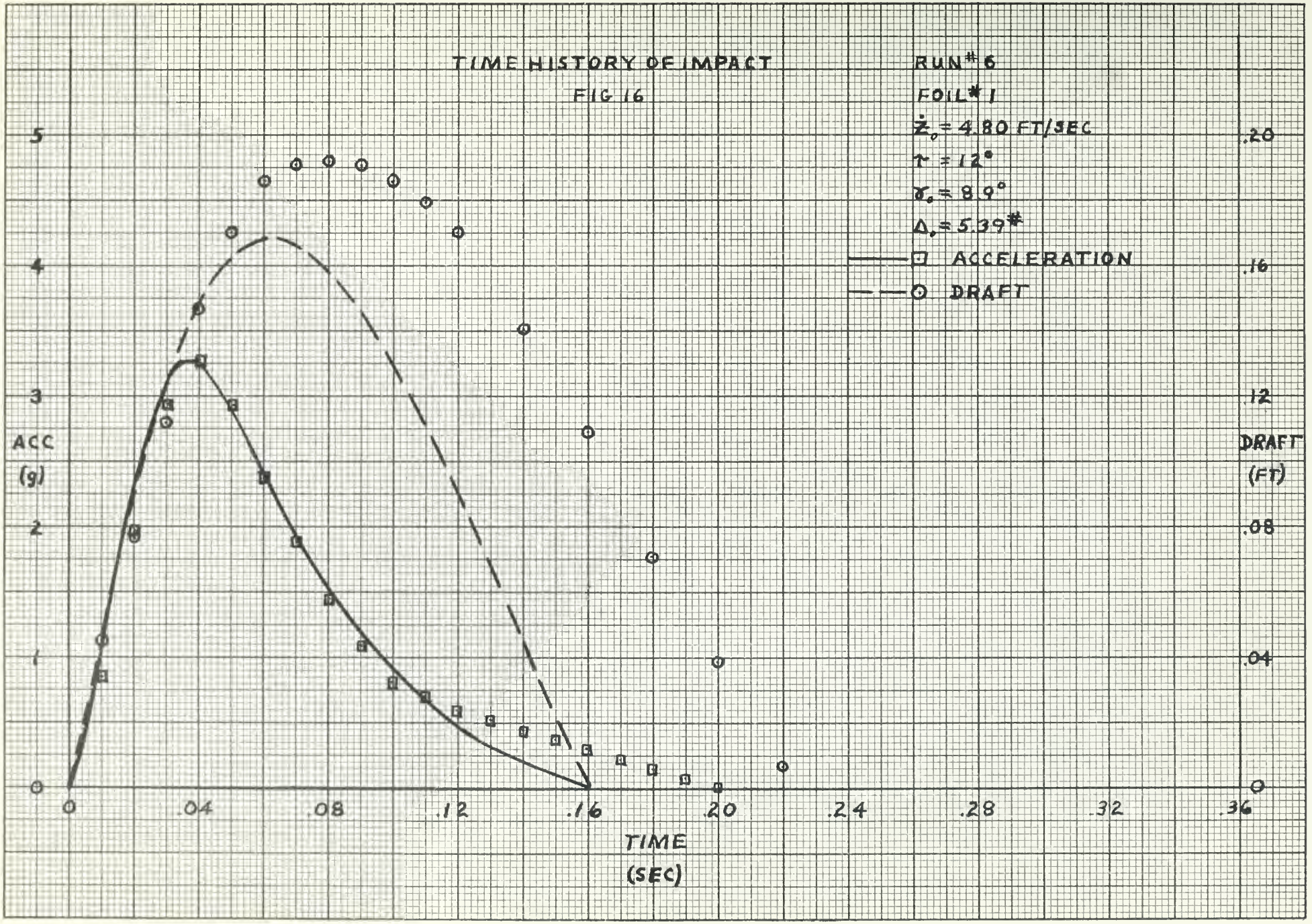
TIME HISTORY OF IMPACT
FIG 16
RUN # 6
FOIL # 1
$\dot{Z}_o$ = 4.80 FT/SEC
τ = 12°
γ_o = 8.9°
Δ_o = 5.39#
ACCELERATION
DRAFT
ACC (g)
DRAFT (FT)
TIME (SEC)
0
1
2
3
4
5
.04
.08
.12
.16
.20
.24
.28
.32
.36
.04
.08
.12
.16
.20

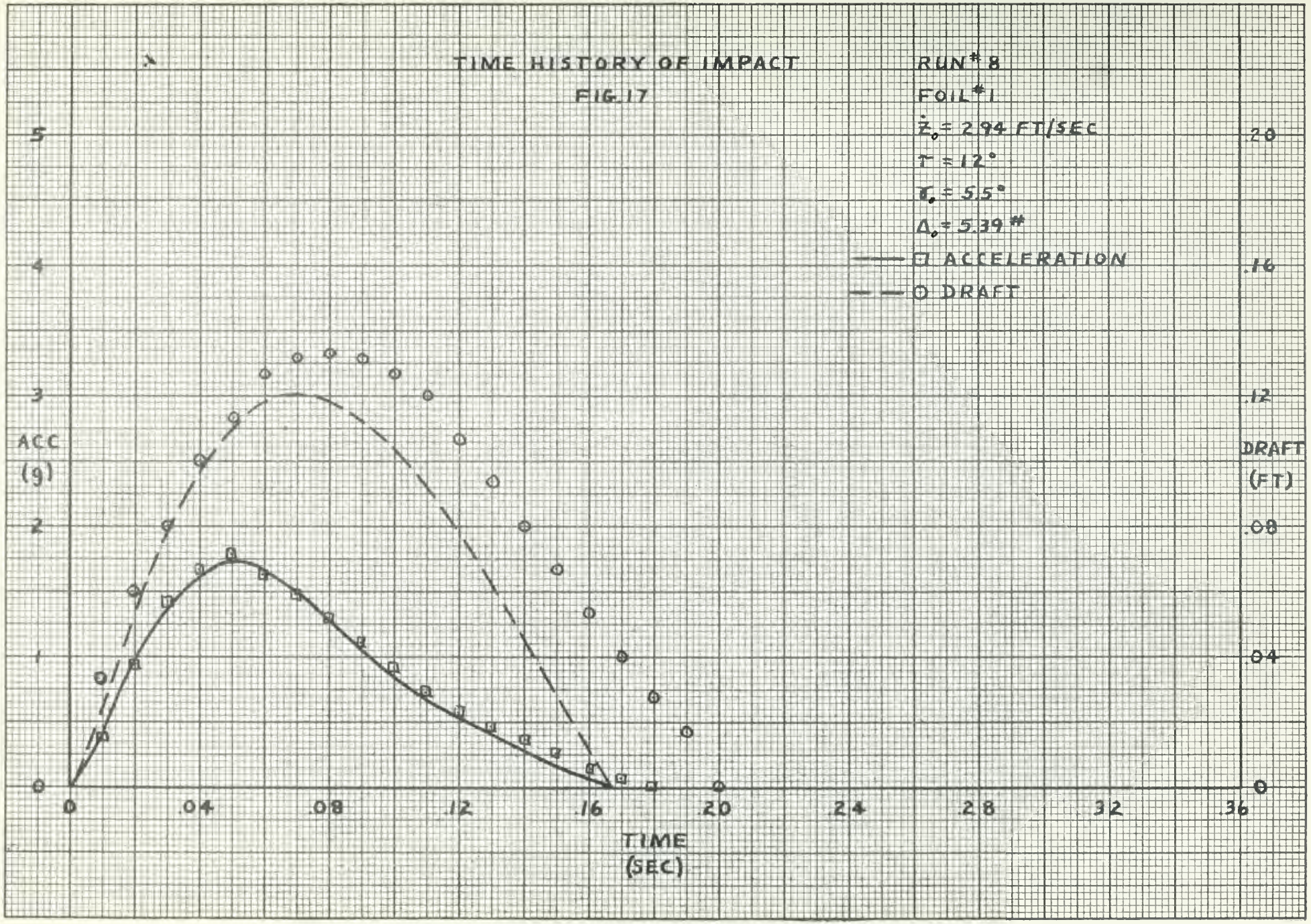
TIME HISTORY OF IMPACT
FIG. 17
RUN # 8
FOIL # 1
$\dot{Z}_0$ = 2.94 FT/SEC
τ = 12°
θ_0 = 5.5°
Δ_0 = 5.39 #
ACCELERATION
DRAFT
ACC (g)
DRAFT (FT)
TIME (SEC)
0
1
2
3
4
5
0
.04
.08
.12
.16
.20
.24
.28
.32
.36
0
.04
.08
.12
.16
.20

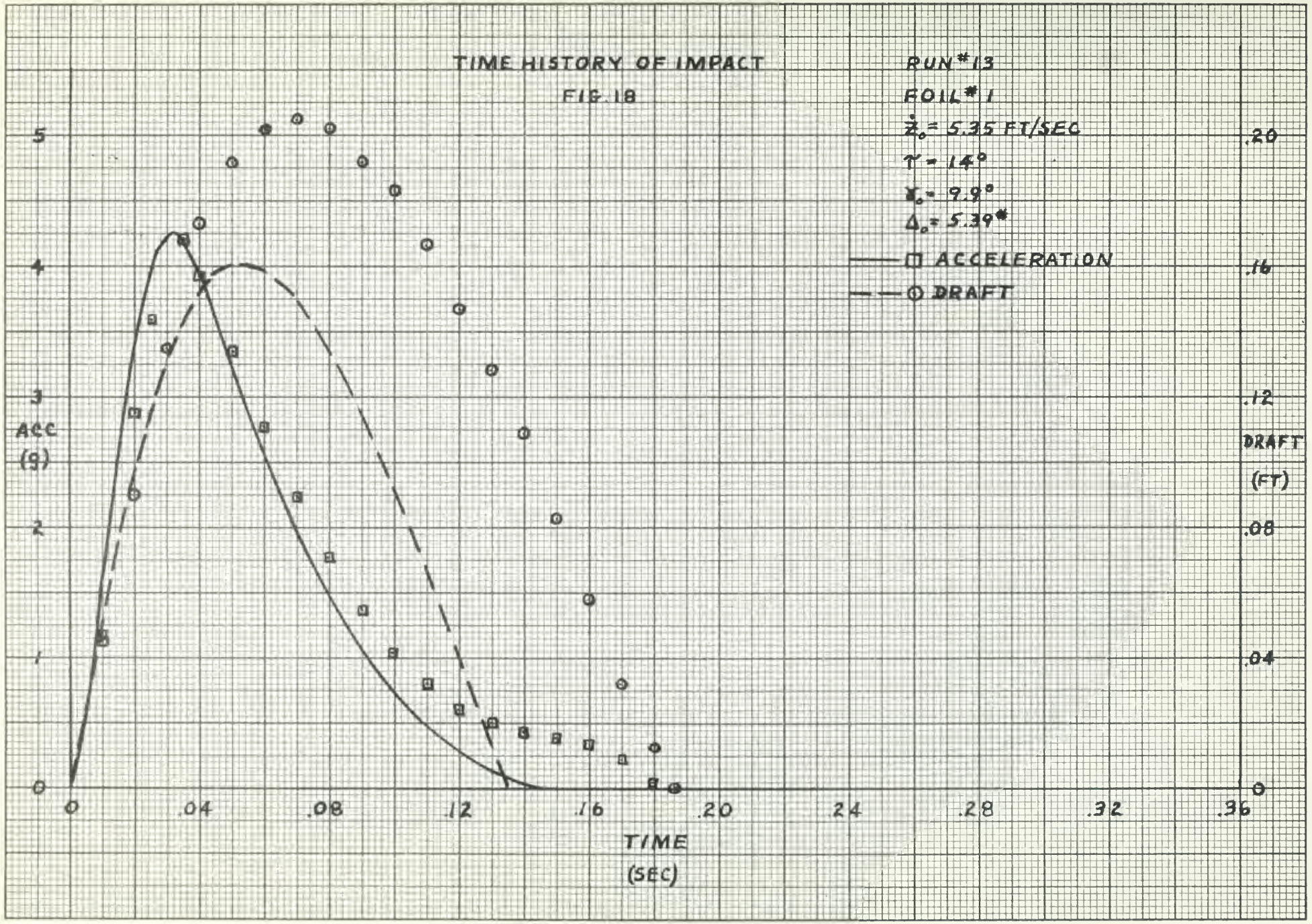
TIME HISTORY OF IMPACT
FIG. 18
RUN # 13
FOIL # 1
$\dot{z}_o$ = 5.35 FT/SEC
τ = 14°
γ_o = 9.9°
Δ_o = 5.39"
ACCELERATION
DRAFT
ACC (g)
DRAFT (FT)
TIME (SEC)
0
1
2
3
4
5
.04
.08
.12
.16
.20
.24
.28
.32
.36
.04
.08
.12
.16
.20

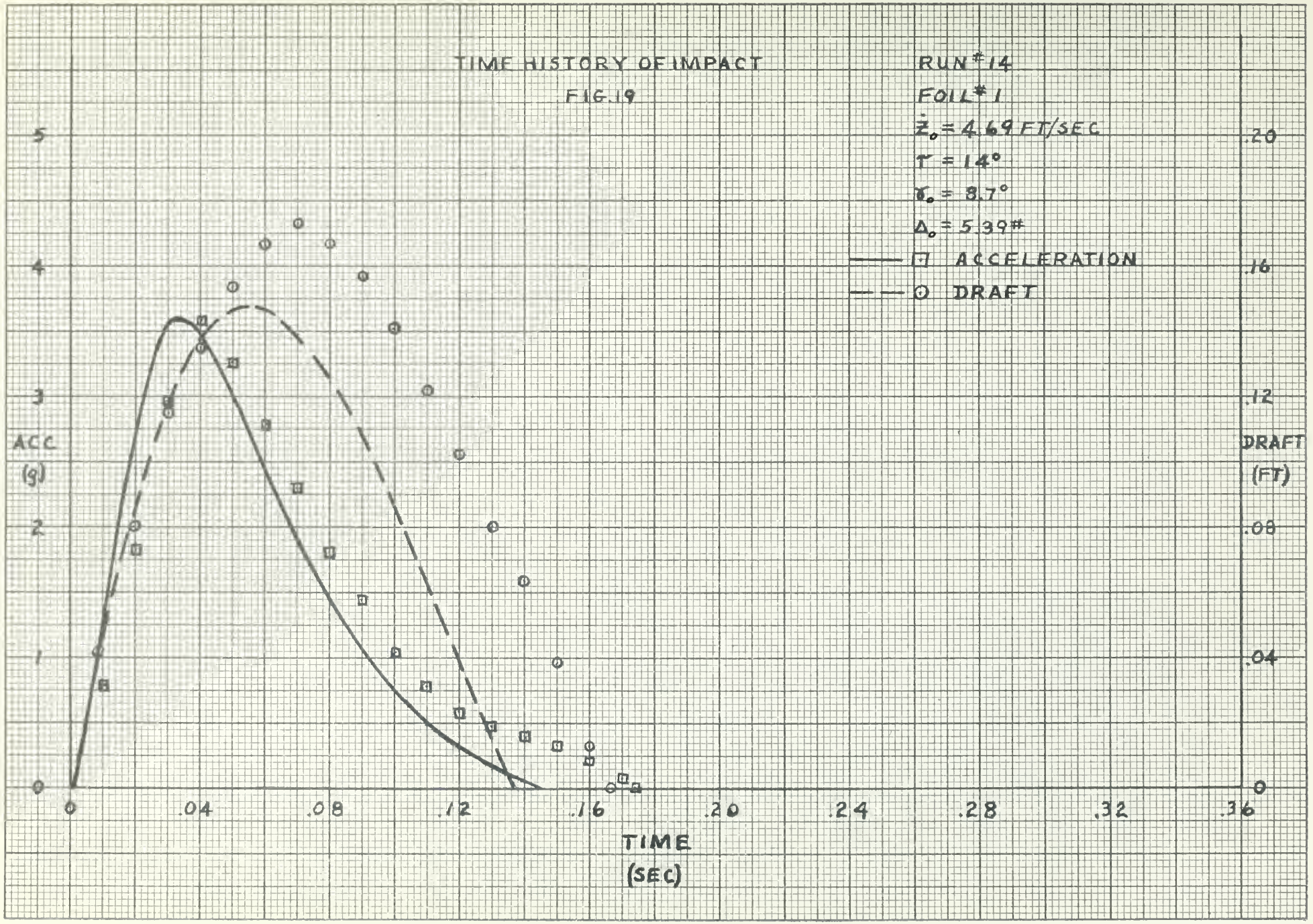
TIME HISTORY OF IMPACT
FIG. 19
RUN # 14
FOIL # 1
$\dot{Z}_o$ = 4.69 FT/SEC
γ = 14°
θ_o = 8.7°
Δ_o = 5.39#
ACCELERATION
DRAFT
ACC (g)
DRAFT (FT)
TIME (SEC)
0
1
2
3
4
5
.04
.08
.12
.16
.20
.24
.28
.32
.36

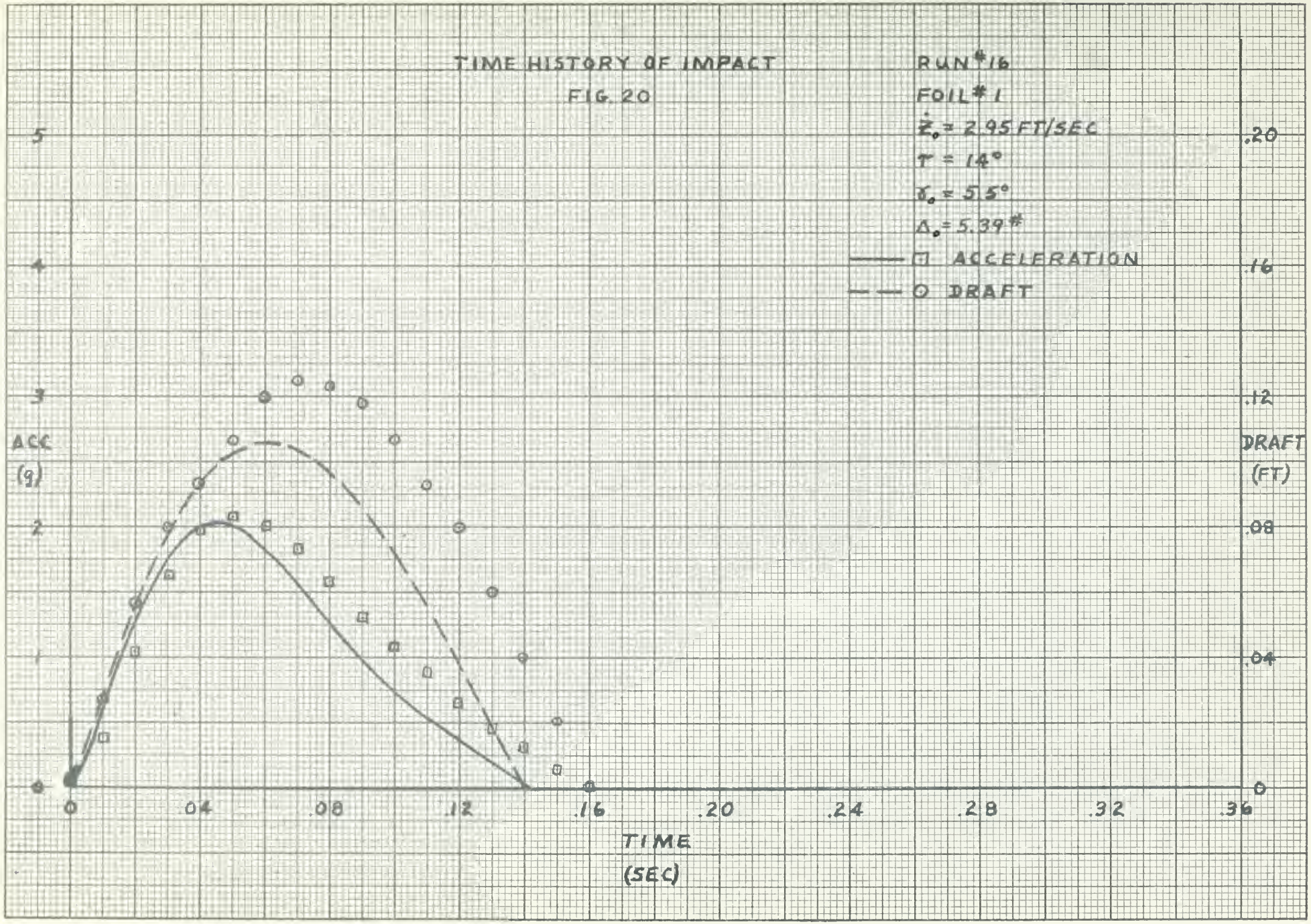
TIME HISTORY OF IMPACT
FIG. 20
RUN #16
FOIL # 1
$\dot{Z}_o$ = 2.95 FT/SEC
τ = 14°
γ_o = 5.5°
Δ_o = 5.39 #
ACCELERATION
DRAFT
ACC (g)
DRAFT (FT)
TIME (SEC)
0
1
2
3
4
5
.04
.08
.12
.16
.20
.24
.28
.32
.36

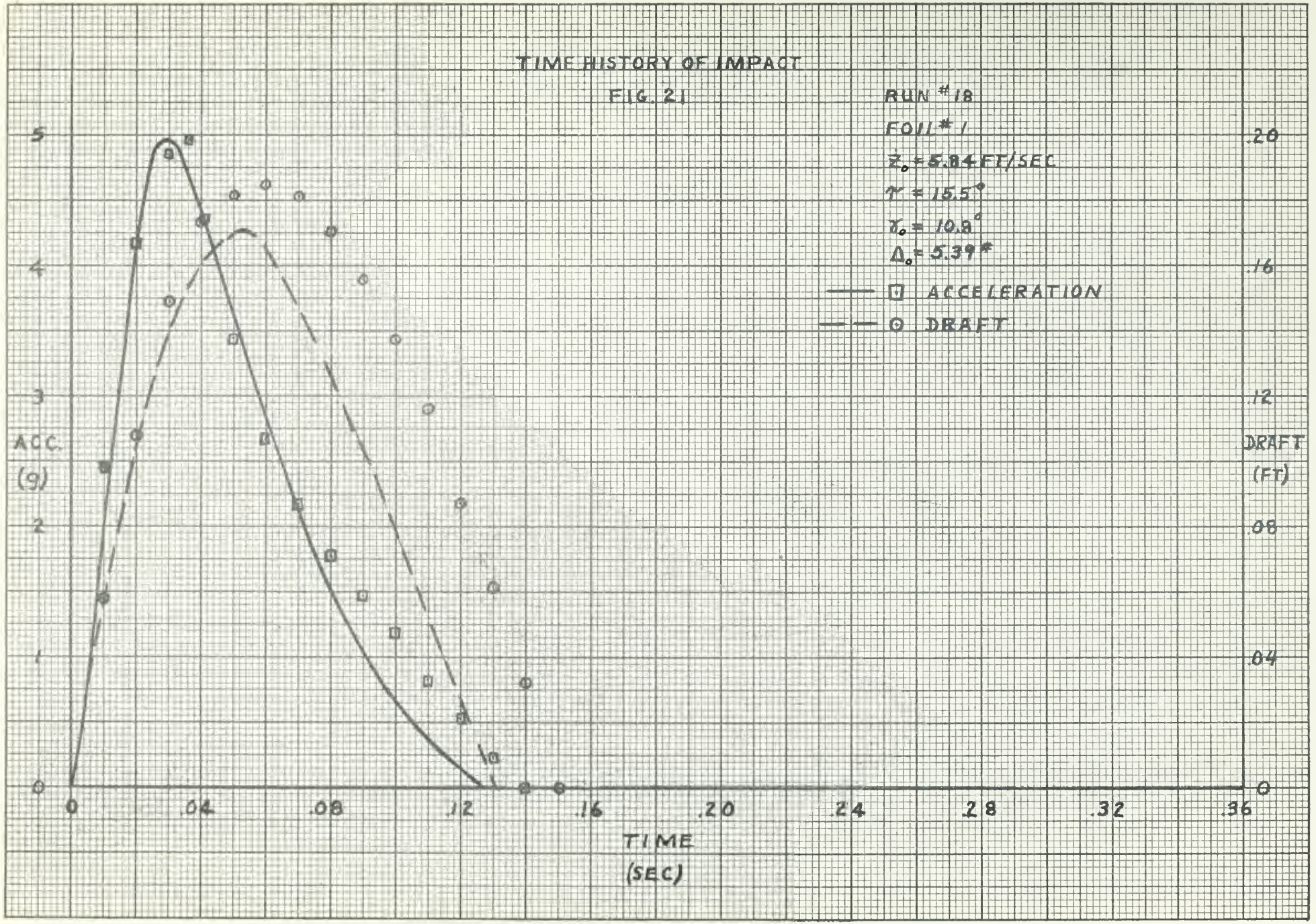
TIME HISTORY OF IMPACT
FIG. 21
RUN # 18
FOIL # 1
$\dot{z}_o$ = 5.84 FT/SEC
γ = 15.5°
γ_o = 10.8°
Δ_o = 5.39 #
ACCELERATION
DRAFT
ACC. (g)
DRAFT (FT)
TIME (SEC)
0
1
2
3
4
5
.04
.08
.12
.16
.20
.24
.28
.32
.36
.04
.08
.12
.16
.20

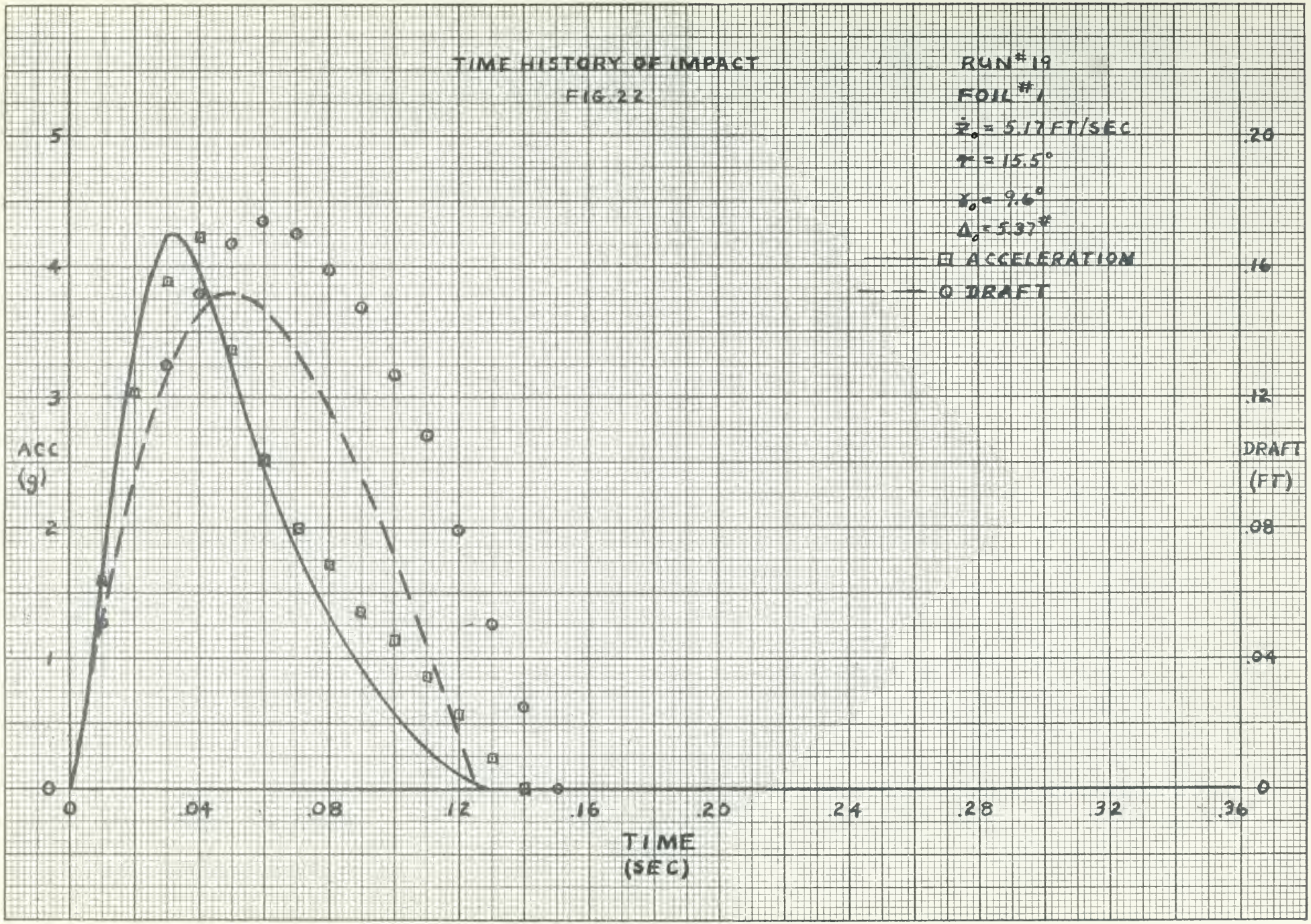
TIME HISTORY OF IMPACT
FIG. 22
RUN # 19
FOIL # 1
$\dot{z}_o$ = 5.17 FT/SEC
τ = 15.5°
γ_o = 9.6°
Δ_o = 5.37"
ACCELERATION
DRAFT
ACC (g)
DRAFT (FT)
TIME (SEC)
0
1
2
3
4
5
.04
.08
.12
.16
.20
.24
.28
.32
.36

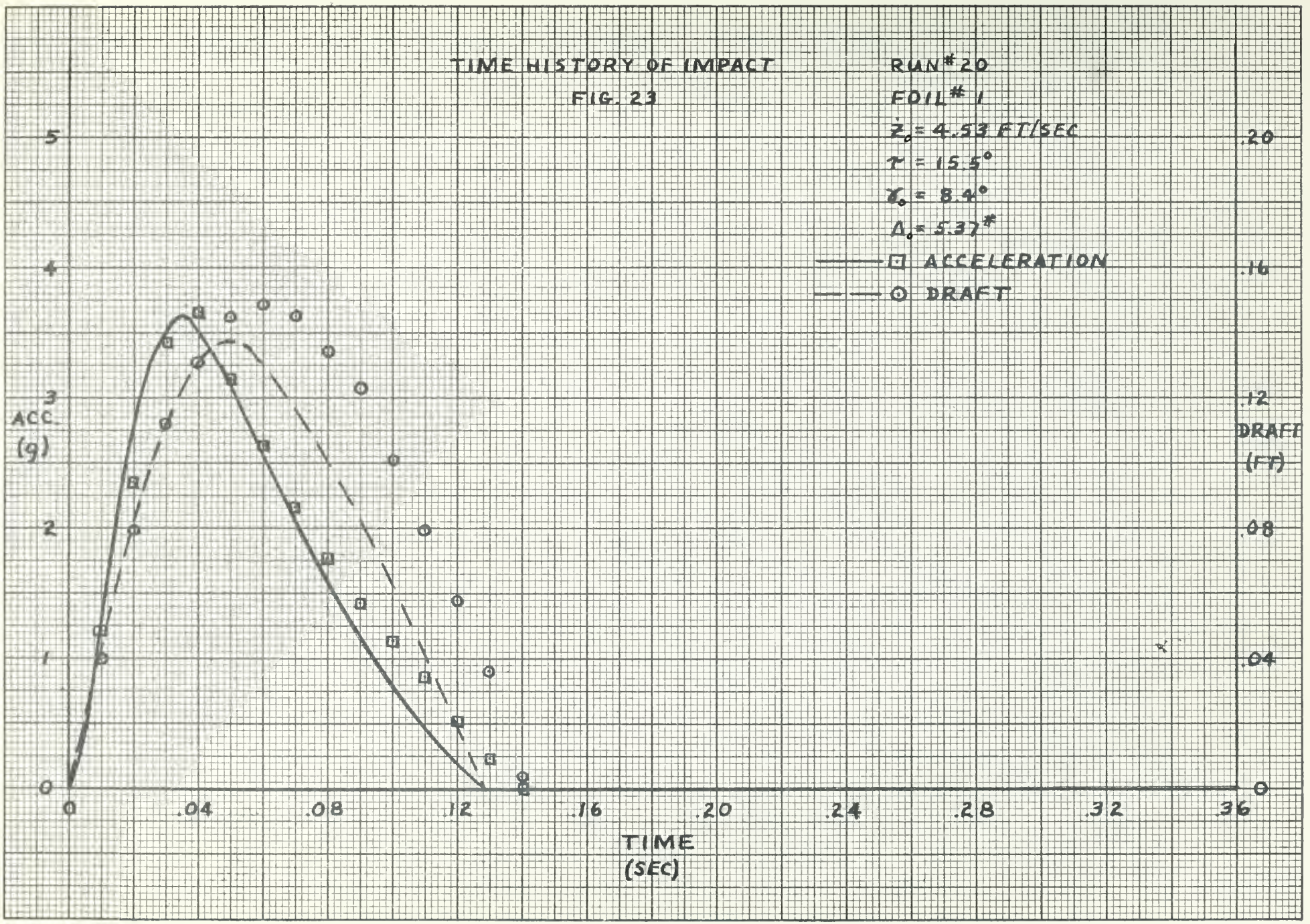
TIME HISTORY OF IMPACT
FIG. 23
RUN # 20
FOIL # 1
$\dot{Z}_o$ = 4.53 FT/SEC
τ = 15.5°
γ_o = 8.4°
Δ_o = 5.37#
ACCELERATION
DRAFT
ACC. (g)
DRAFT (FT)
TIME (SEC)
0
1
2
3
4
5
.04
.08
.12
.16
.20
.24
.28
.32
.36

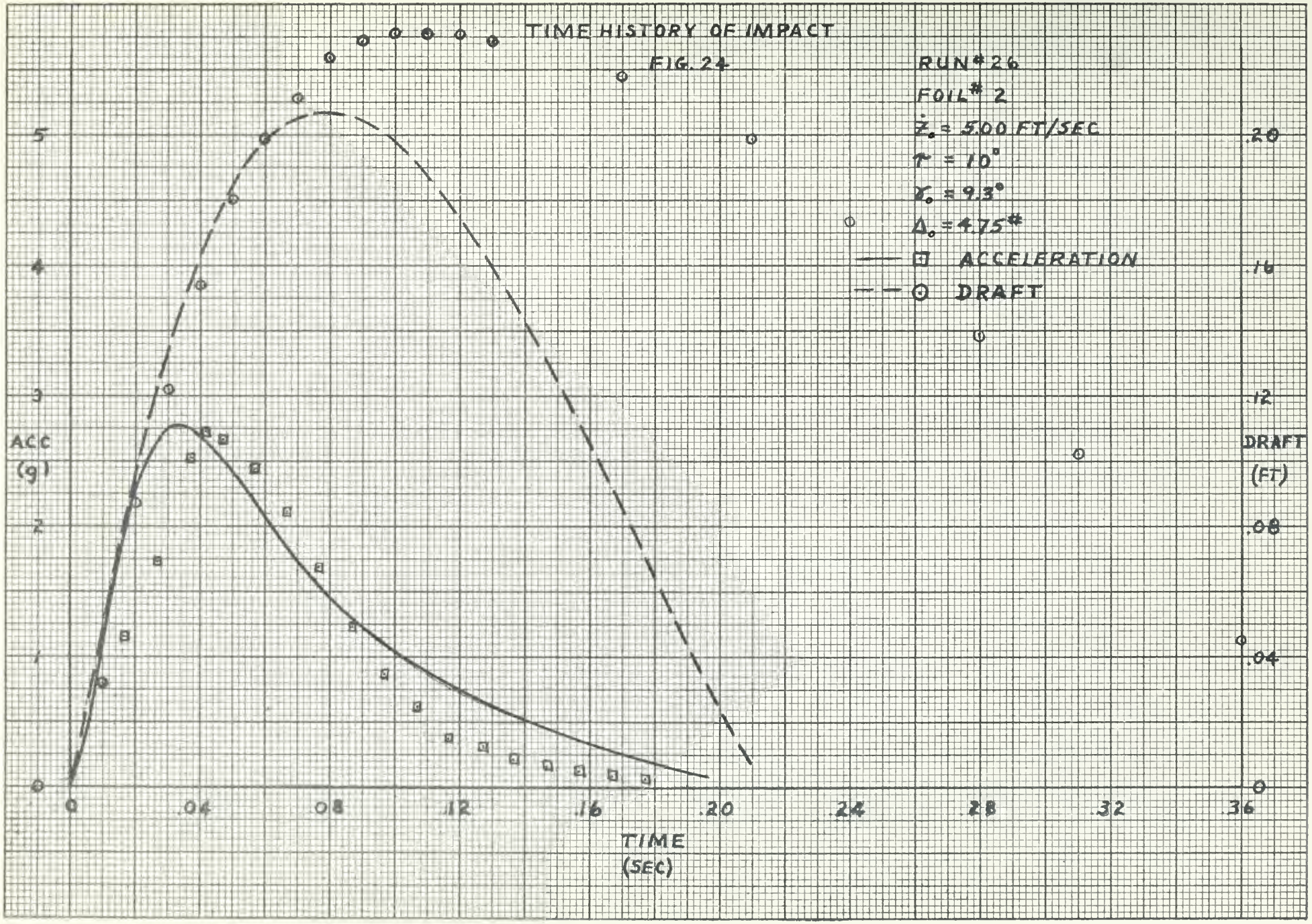
TIME HISTORY OF IMPACT
FIG. 24
RUN # 26
FOIL # 2
$\dot{Z}_o$ = 5.00 FT/SEC
τ = 10°
γ_o = 9.3°
Δ_o = 4.75#
ACCELERATION
DRAFT
ACC (g)
DRAFT (FT)
TIME (SEC)
0
1
2
3
4
5
.04
.08
.12
.16
.20
.24
.28
.32
.36

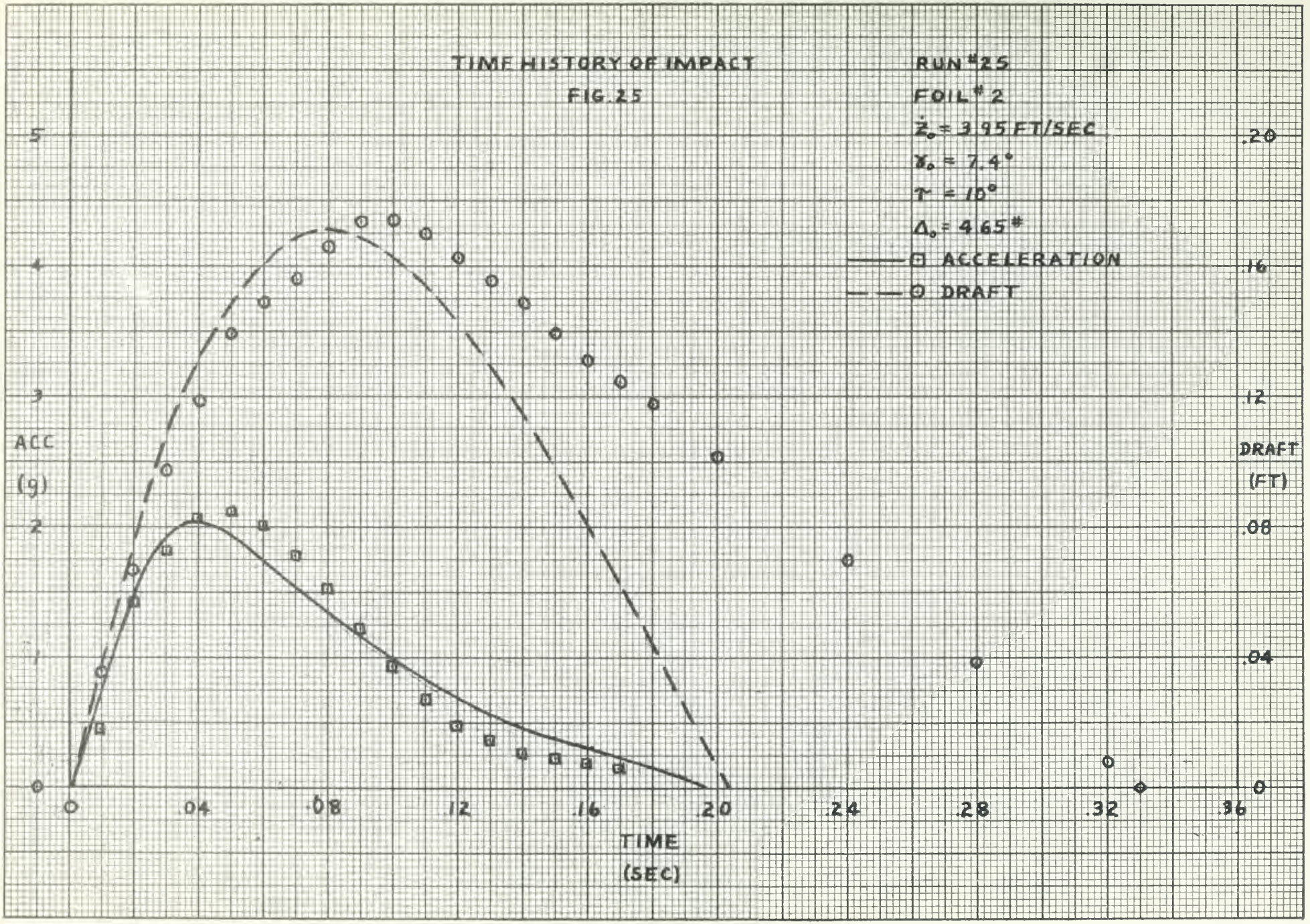
TIME HISTORY OF IMPACT
FIG. 25
RUN # 25
FOIL # 2
$\dot{Z}_o$ = 3.95 FT/SEC
γ_o = 7.4°
τ = 10°
Δ_o = 4.65 #
ACCELERATION
DRAFT
ACC (g)
DRAFT (FT)
TIME (SEC)
0
1
2
3
4
5
.04
.08
.12
.16
.20
.24
.28
.32
.36
.04
.08
.12
.16
.20

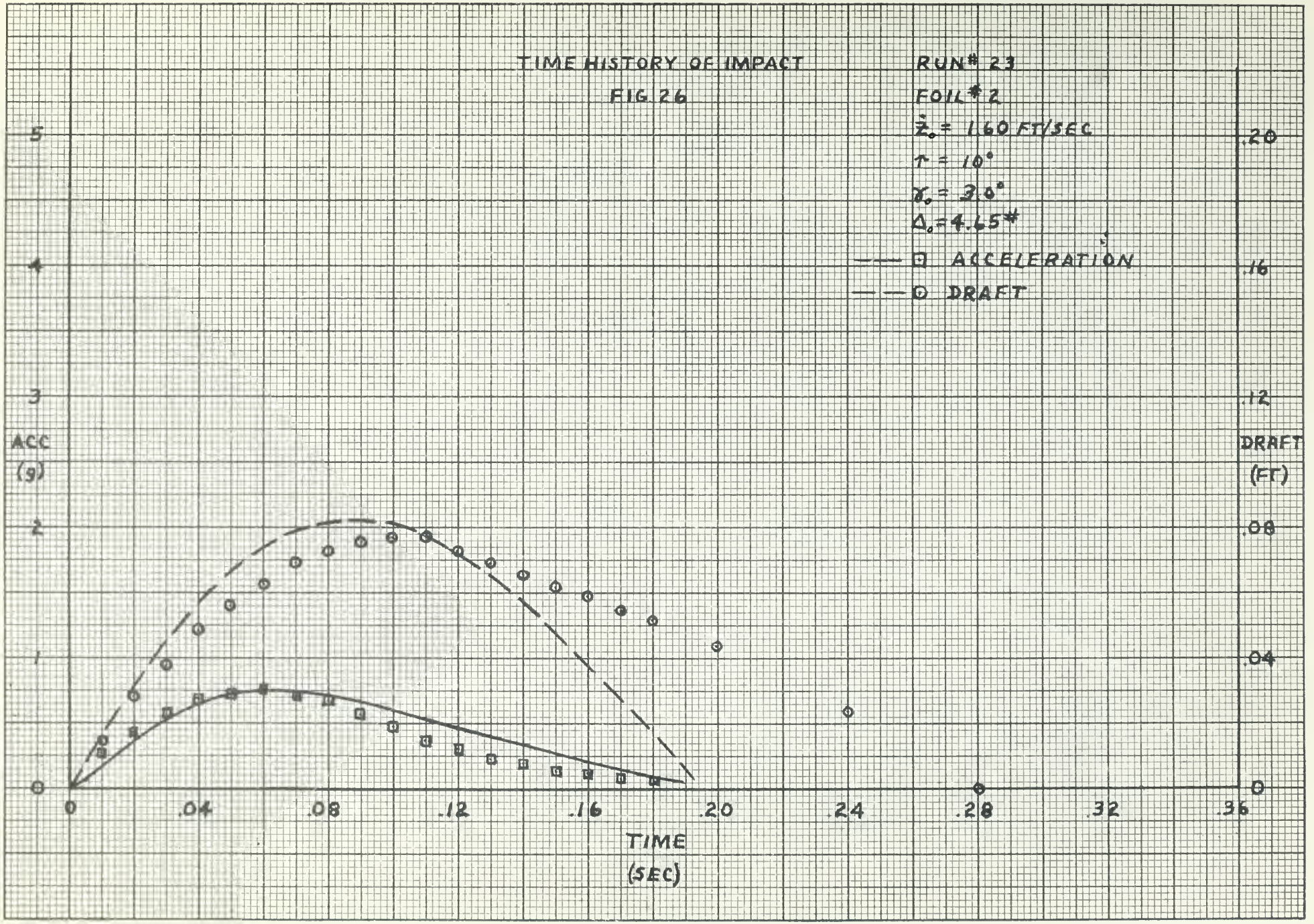
TIME HISTORY OF IMPACT
FIG. 26
RUN # 23
FOIL # 2
$\dot{z}_o$ = 1.60 FT/SEC
τ = 10°
γ_o = 3.0°
Δ_o = 4.65#
ACCELERATION
DRAFT
ACC (g)
DRAFT (FT)
TIME (SEC)
0
1
2
3
4
5
0
.04
.08
.12
.16
.20
.24
.28
.32
.36
0
.04
.08
.12
.16
.20

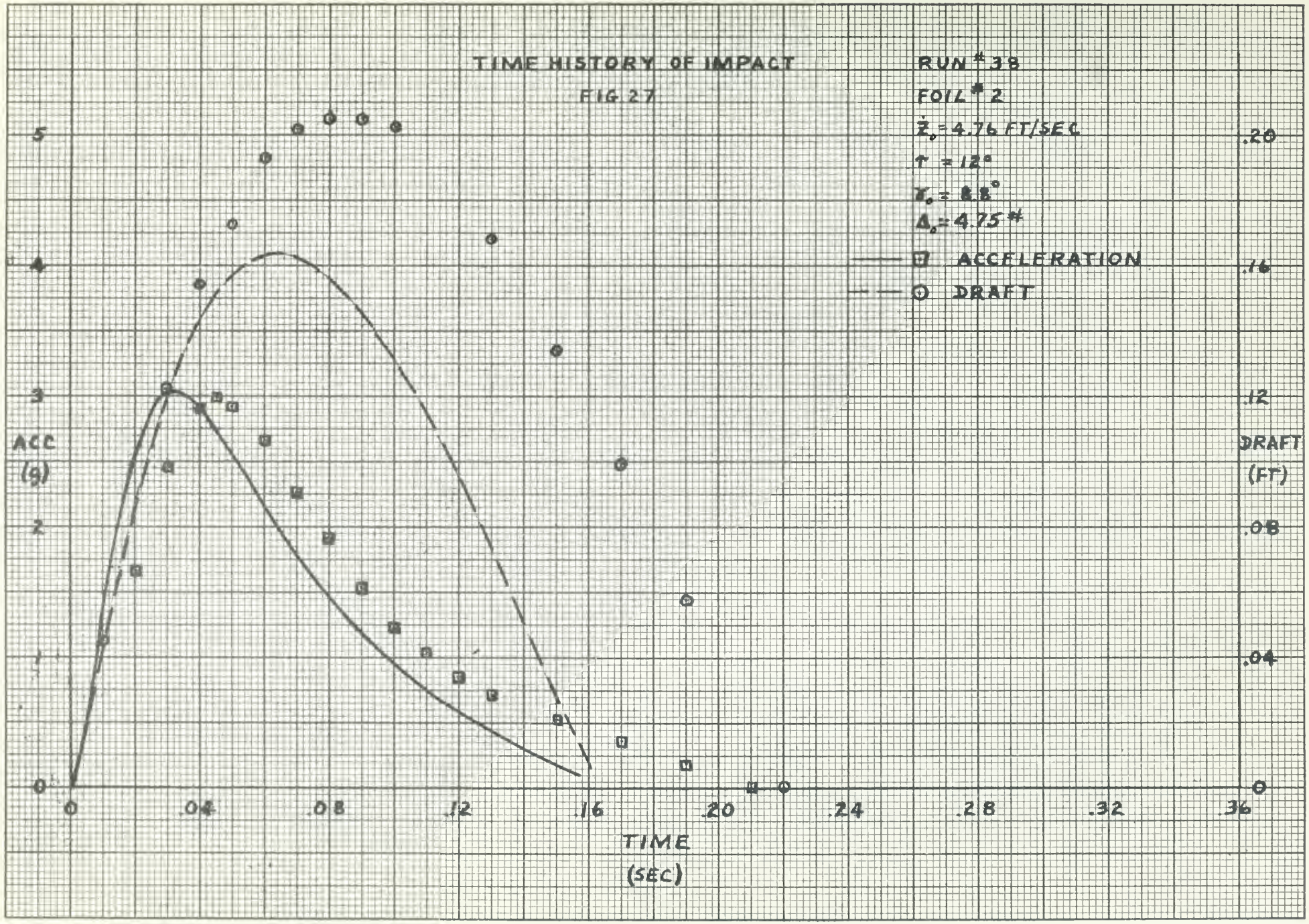
TIME HISTORY OF IMPACT
FIG 27
RUN # 38
FOIL # 2
$\dot{Z}_o$ = 4.76 FT/SEC
τ = 12°
γ_o = 8.8°
Δ_o = 4.75 #
ACCELERATION
DRAFT
ACC (g)
DRAFT (FT)
TIME (SEC)
0
1
2
3
4
5
.04
.08
.12
.16
.20
.24
.28
.32
.36
.04
.08
.12
.16
.20

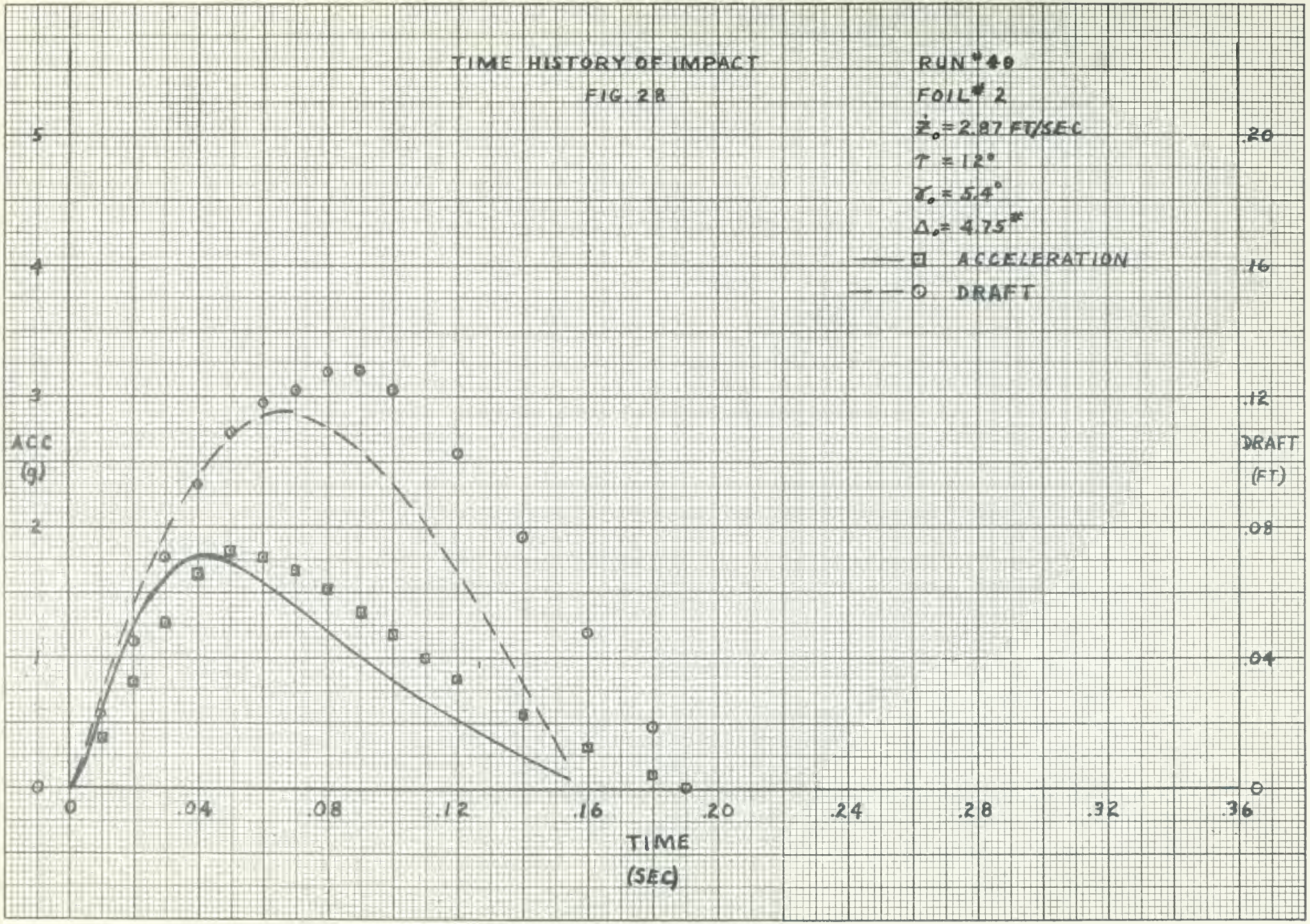
TIME HISTORY OF IMPACT
FIG. 28
RUN # 40
FOIL # 2
$\dot{z}_o$ = 2.87 FT/SEC
τ = 12°
γ_o = 5.4°
Δ_o = 4.75#
ACCELERATION
DRAFT
ACC (g)
DRAFT (FT)
TIME (SEC)
0
1
2
3
4
5
.04
.08
.12
.16
.20
.24
.28
.32
.36
.04
.08
.12
.16
.20

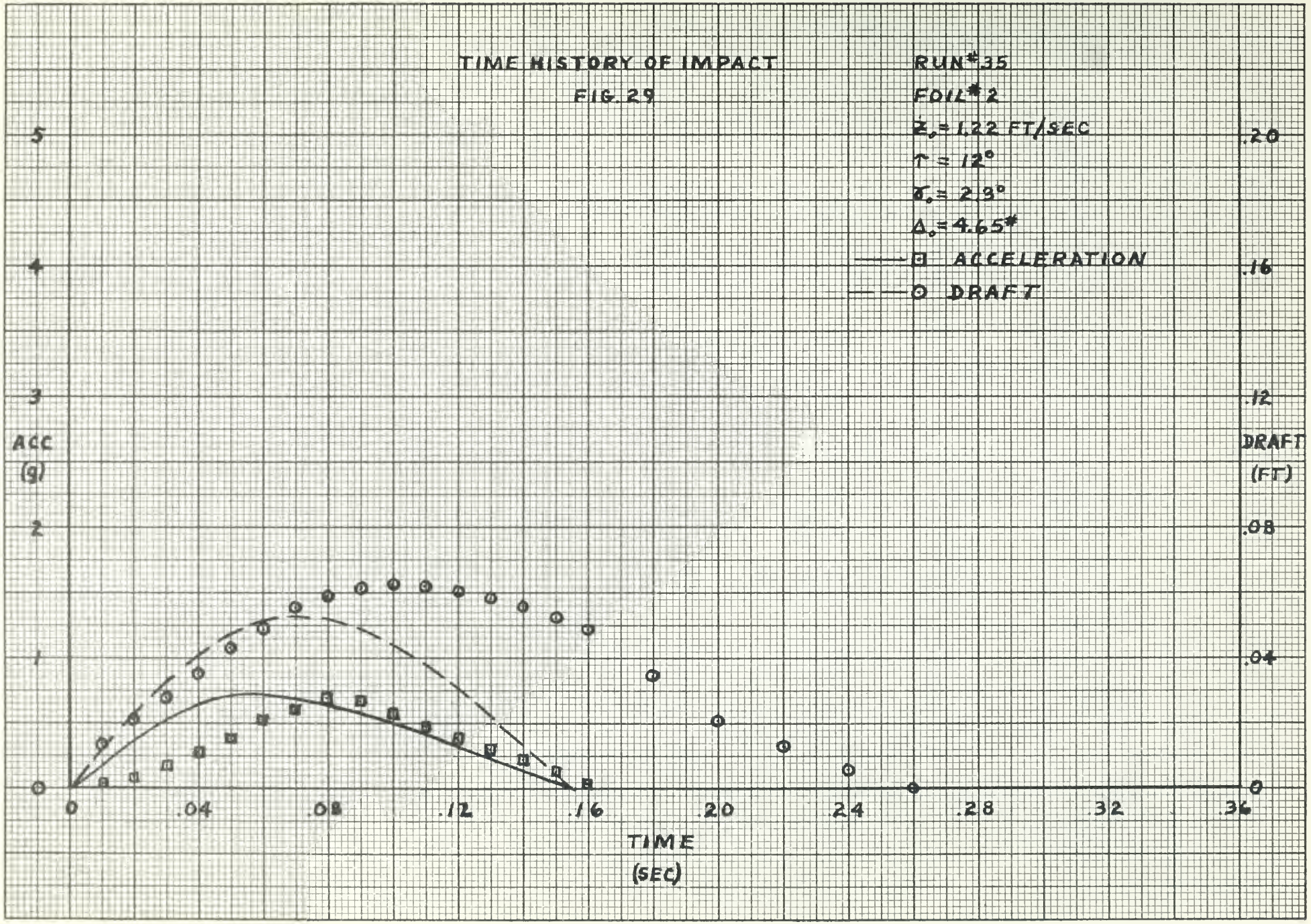
TIME HISTORY OF IMPACT
FIG. 29
RUN # 35
FOIL # 2
V_o = 1.22 FT/SEC
τ = 12°
σ_o = 2.3°
Δ_o = 4.65#
ACCELERATION
DRAFT
ACC (g)
DRAFT (FT)
TIME (SEC)
0
1
2
3
4
5
.04
.08
.12
.16
.20
.24
.28
.32
.36
.20
.16
.12
.08
.04
0

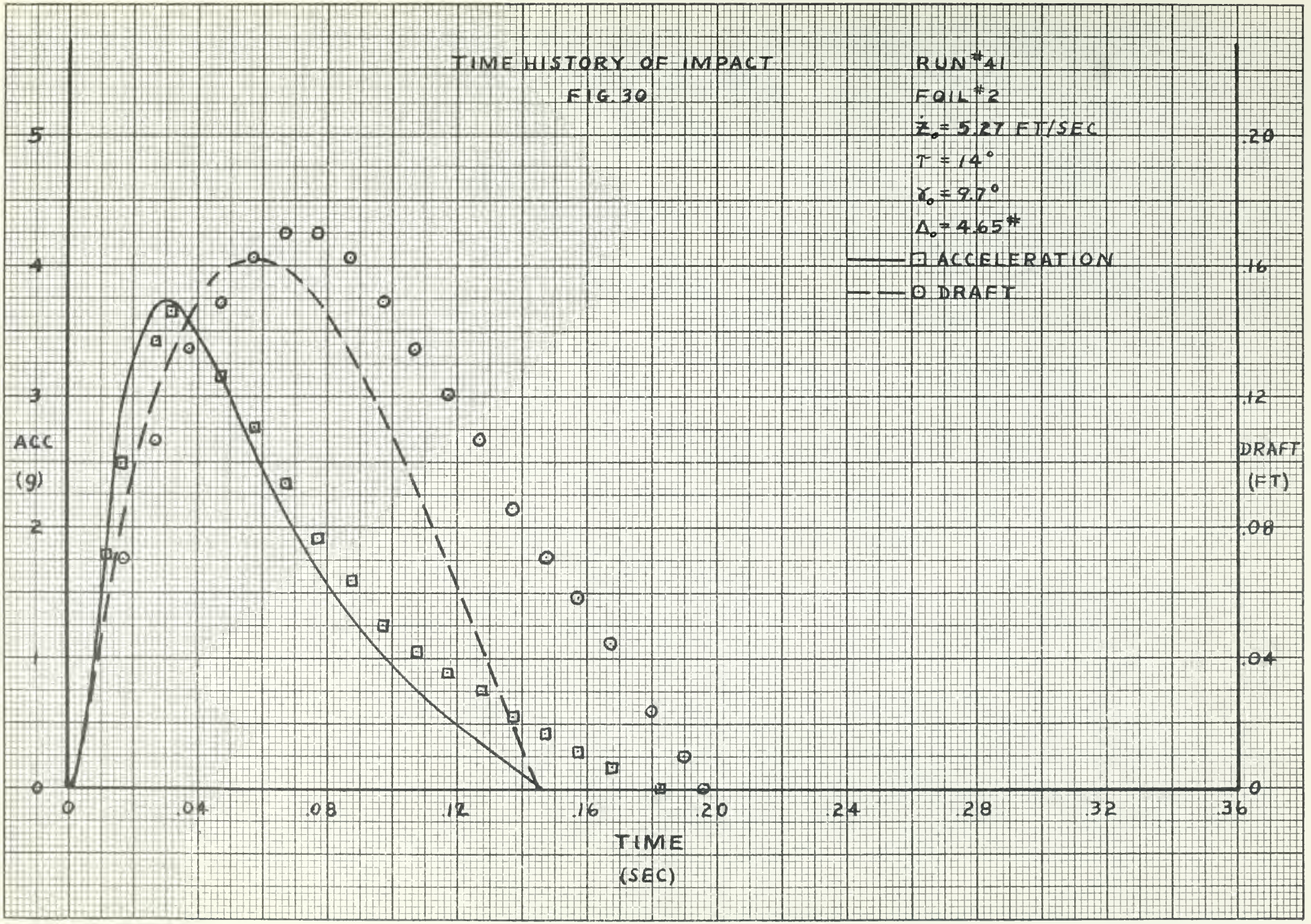
TIME HISTORY OF IMPACT
FIG. 30
RUN #41
FOIL #2
$\dot{Z}_o$ = 5.27 FT/SEC
τ = 14°
γ_o = 9.7°
Δ_o = 4.65#
ACCELERATION
DRAFT
ACC (g)
DRAFT (FT)
TIME (SEC)
0
1
2
3
4
5
.04
.08
.12
.16
.20
.24
.28
.32
.36

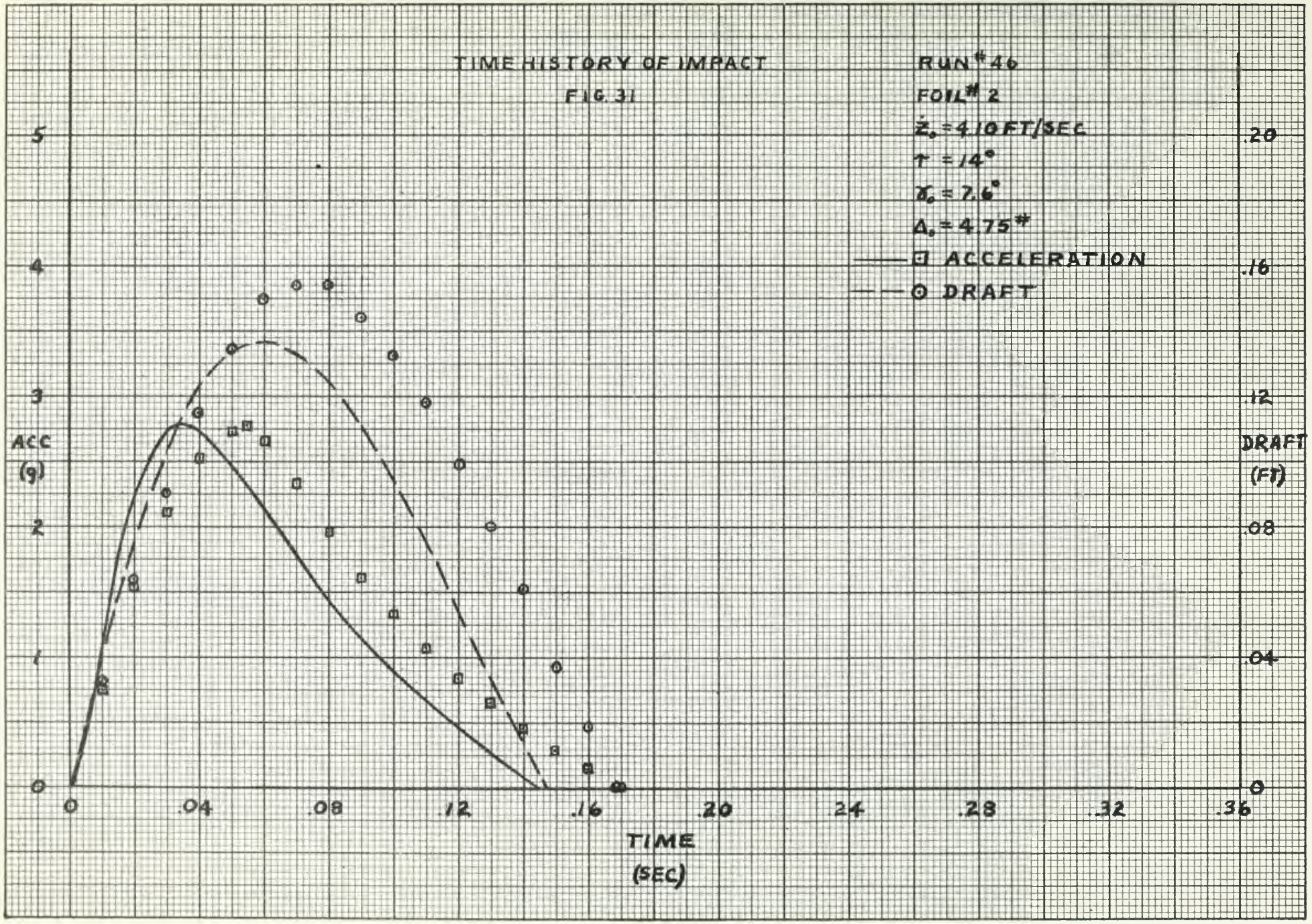
TIME HISTORY OF IMPACT
FIG. 31
RUN # 46
FOIL # 2
$\dot{Z}_o$ = 4.10 FT/SEC
τ = 14°
γ_c = 7.6°
Δ_o = 4.75 #
ACCELERATION
DRAFT
ACC (g)
DRAFT (FT)
TIME (SEC)
0
1
2
3
4
5
.04
.08
.12
.16
.20
.24
.28
.32
.36
.04
.08
.12
.16
.20

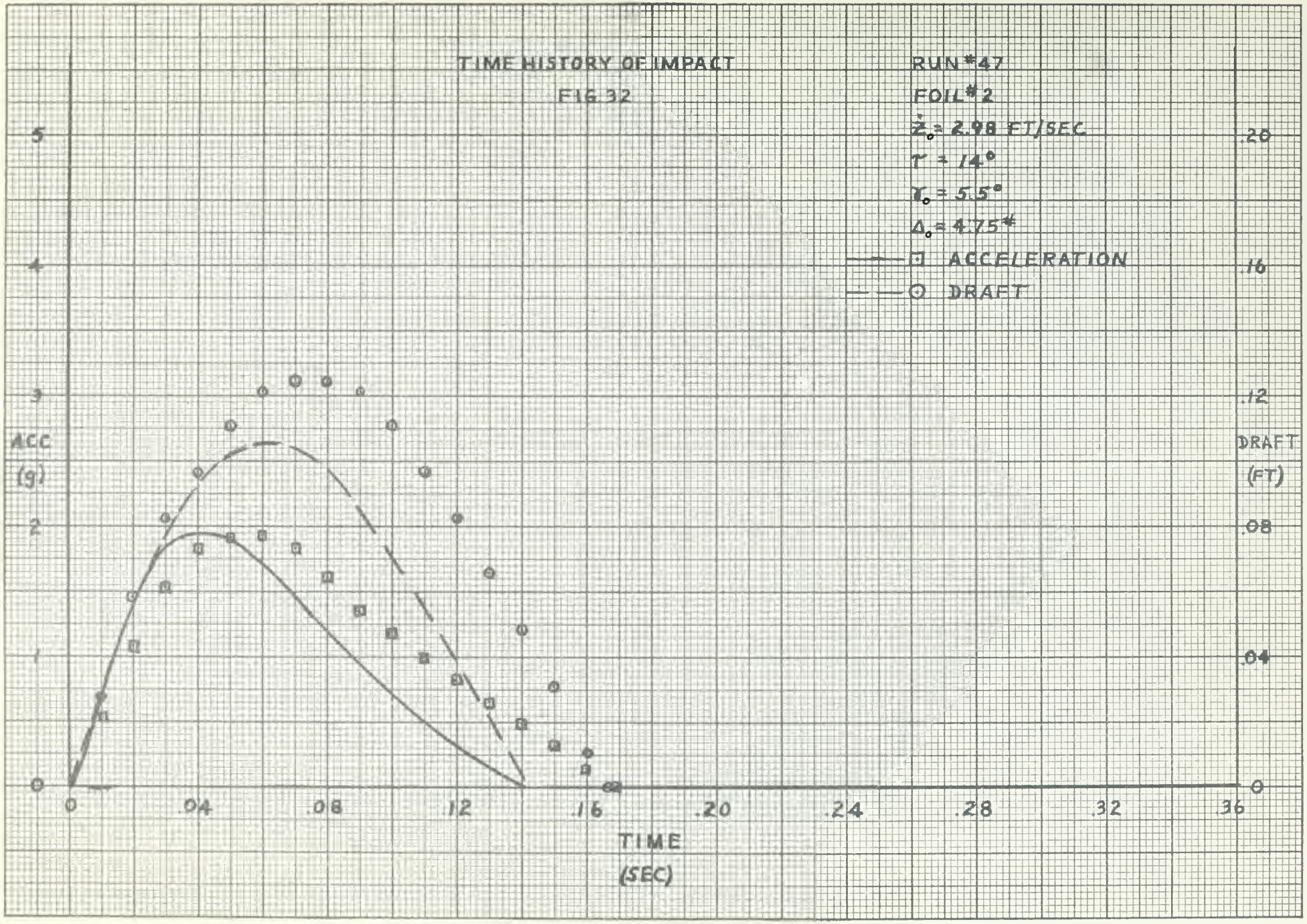
TIME HISTORY OF IMPACT
FIG 32
RUN #47
FOIL #2
$\dot{z}_o$ = 2.98 FT/SEC
τ = 14°
γ_o = 5.5°
Δ_o = 4.75#
ACCELERATION
DRAFT
ACC (g)
DRAFT (FT)
TIME (SEC)
0
1
2
3
4
5
0
.04
.08
.12
.16
.20
.24
.28
.32
.36
0
.04
.08
.12
.16
.20

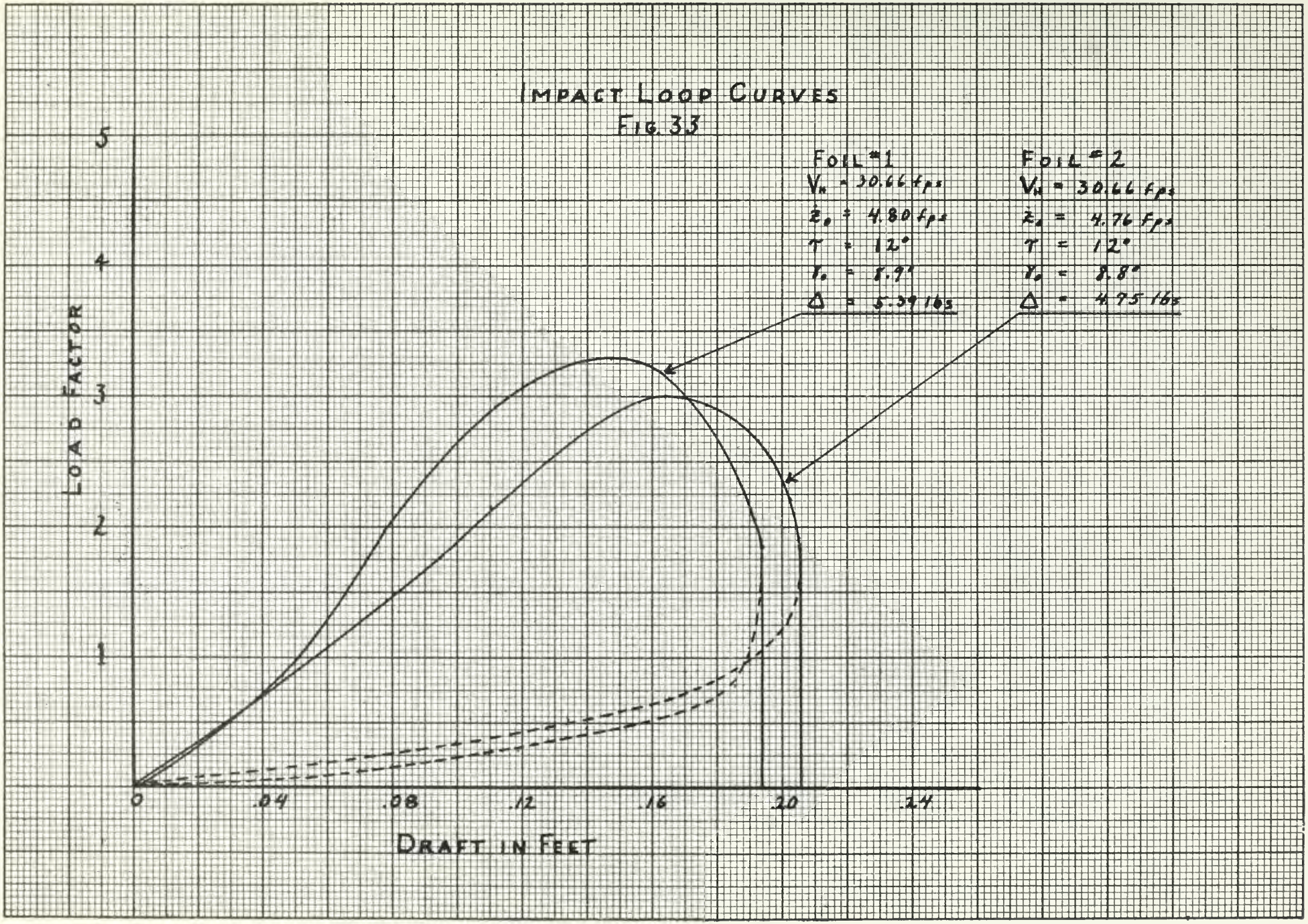
IMPACT LOOP CURVES
FIG. 3.3
FOIL #1
V_H = 30.66 fps
$\dot{z}_0$ = 4.80 fps
τ = 12°
γ_0 = 8.9°
Δ = 5.39 lbs
FOIL #2
V_H = 30.66 fps
$\dot{z}_0$ = 4.76 fps
τ = 12°
γ_0 = 8.8°
Δ = 4.95 lbs
LOAD FACTOR
1
2
3
4
5
0
.04
.08
.12
.16
.20
.24
DRAFT IN FEET

Thesis
H673
c.1

35883

Hoffman

A study of the hydrodynamic impact loads on a dihedral hydro foil suitable for seaplane use.